Generation and characterization of entangled photons source through spontaneous parametric down conversion

A Thesis

submitted to
Indian Institute of Science Education and Research Pune
in partial fulfillment of the requirements for the
BS-MS Dual Degree Programme

by

Chandana Rao A S

Indian Institute of Science Education and Research Pune
Dr. Homi Bhabha Road,
Pashan, Pune 411008, INDIA.

April, 2023

Supervisor: Prof. Umakant D Rapol

Certificate

This is to certify that this dissertation entitled Generation and characterization of entangled photons source through spontaneous parametric down conversion towards the partial fulfilment of the BS-MS dual degree programme at the Indian Institute of Science Education and Research, Pune represents study/work carried out by Chandana Rao A S at Indian Institute of Science Education and Research under the supervision of Prof. Umakant D Rapol, Professor, Department of Physics , during the academic year 2022-2023.

Prof. Umakant D Rapol

Committee:

Prof. Umakant D Rapol

Dr. Anindita B

Prof. M S Santhanam

This thesis is dedicated to Prof. Umakant D Rapol for providing invaluable mentorship over the past 5 years.

Declaration

I hereby declare that the matter embodied in the report entitled Generation and characterization of entangled photons source through spontaneous parametric down conversion are the results of the work carried out by me at the Department of Physics, Indian Institute of Science Education and Research, Pune, under the supervision of Prof. Umakant D Rapol and the same has not been submitted elsewhere for any other degree.

Chandana Rao A S

Acknowledgments

I am deeply grateful to Prof. Umakanth D Rapol for his invaluable guidance and mentorship throughout the past 5 years of my academic pursuit. His vast knowledge, expertise, and constructive feedback have shaped my academic journey, and I am thankful for his constant support. I am thankful to Dr. Anindita B, Adjunct Scientist, Centre for Development of Advanced Computing (C-DAC) Pune, for giving me an opportunity to do an internship in C-DAC, Pune and her insightful inputs for the better outcome of my project. I thank Prof. G Raghavan, Director of School of Quantum Technology, Defence Institute Of Advanced Technology, Pune for permitting me to use the required tools for conducting my experiments. I thank Prof. M S Santhanam for providing timely assistance and guidance during the completion of this project. I sincerely thank my parents and godmother for their unwavering moral support.

Contents

List of Figures

List of Tables

Abstract

This thesis explores the generation and characterization of entangled photons source using a type-1 crossed Beta-Barium Borate (BBO) crystal through the spontaneous parametric down conversion (SPDC), with a focus on understanding the quantum entanglement phenomenon and its application in quantum information and communication. Various experimental tests, including Hanbury Brown and Twiss (HBT) experiment, visibility, Clauser-Horne-Shimony-Holt (CHSH) inequality, and polarization correlation measurements, were conducted to characterize the entangled photons source. Additionally, the quantum state tomography technique was used to reconstruct the density matrix of the entangled photons. The results show that the source generates moderately entangled, single photons, which violate the Bell inequality as evidenced by the CHSH parameter of 2.629±0.021. The concurrence value of 0.708 and linear entropy of 0.244 provide estimates of the degree of entanglement and noise present in the entangled photons, respectively.

Introduction

Entanglement is a fundamental concept in quantum mechanics, wherein the properties of multiple particles become correlated to such an extent that their states are no longer independent of each other. This strange phenomenon, famously referred to as "spooky action at a distance" by Einstein [1], has been confirmed by plethora of experiments such as the Bell test experiments (1964) [2], the Aspect experiment (1982) [3] the Weihs experiment (1998) [4] and many more, with profound implications for our understanding of reality.

Given the potential of entangled photons to enable secure communication and powerful computational methods, they have become a vital component in contemporary quantum technologies. A comprehensive understanding of the properties and behavior of entangled photons is therefore essential for developing novel quantum technologies and advancing fundamental physics. Thus far, entangled photons have been utilized in a diverse range of applications such as quantum teleportation [5, 6] where the quantum state of one particle is transferred to another without physically moving the particle; in quantum cryptography [7, 8], entangled photons create secure communication channels by detecting any attempt at interception or eavesdropping. They are also used as quantum bits in quantum computing to process information faster than classical computers and in precision measurement applications such as interferometry for detecting tiny changes in position or time, making them useful in gravitational wave detection [9, 10]. Quantum ghost imaging [13, 14] utilizes entangled photons to create high-resolution images by analyzing correlations between two photons.

One of the approaches to generating entangled photons is by exploiting the nonlinear response of certain materials during the interaction between incident light and matter. These are the nonlinear optical processes that have garnered significant attention due to their crucial role in diverse applications such as optical communication, microscopy, and quantum computing. Unlike linear optical processes, nonlinear effects stem from changes to the medium's dielectric properties caused by the applied field, resulting in the generation of new frequencies or the modification of the incident radiations [15].

The goal of this master's thesis is to investigate the process of generating and characterizing entangled photons source through spontaneous parametric down conversion [16, 17, 24], a promising method with significant potential to advance quantum technology. The sensitivity of this process to experimental parameters, such as crystal properties and pump power, presents a significant

challenge. By analyzing the properties of entangled photon pairs and optimizing experimental conditions, this research aims to contribute to the quantum key distribution protocols while furthering our understanding of quantum entanglement.

In this work, we focus on the generation and characterization of entangled photons source using a crossed type-1 Beta-Barium Borate (BBO) crystal. The experimental setup involves the use of a high power UV diode laser at 405 nm wavelength as the pump source to generate entangled photon pairs of 810nm in the crystal.

To characterize the entangled photon source, we performed a series of experiments such as the Hanbury-Brown and Twiss (HBT) experiment [18], CHSH inequality [19], visibility [21], polarization correlation measurements[23] and quantum state tomography [22]. The HBT experiment was used to study the photon statistics of the source. The CHSH inequality, polarization correlation measurements and visibility experiments were used to verify the entanglement and to quantify the degree of entanglement. Finally, the quantum state tomography experiment was used to reconstruct the density matrix of the entangled photon pairs.

This thesis is organised into 5 chapters as follows:

- **Chapter 1:** It provides a theoretical explanation of nonlinear optical processes, with a focus on the optics of nonlinear crystals and the SPDC process. It covers mathematical derivations of the nonlinear equations governing the behavior of nonlinear crystals and discusses the SPDC process and its relevance in generation of entangled photons. It also explains the concept of phase matching, which is essential for achieving efficient nonlinear frequency conversion.
- **Chapter 2:** Presents a comprehensive theoretical study of different schemes for generating entangled photons using nonlinear crystals. The chapter covers Type-0, Type-I and Type-II phase matching schemes through SPDC using bulk and periodically poled crystals. For each scheme, the chapter provides a detailed explanation of the underlying theoretical principles, along with corresponding schematics.
- **Chapter 3:** Here, we focus on the experimental characterization of entangled photons. Specifically, we investigate the brightness of the entangled photon source, the heralding efficiency, the Hanbury Brown and Twiss (HBT) experiment, the violation of the Clauser-Horne-Shimony-Holt (CHSH) inequality, the visibility of the interference fringes, the polar-

ization correlation measurements, and the reconstruction of the quantum state using quantum state tomography. Detailed theoretical explanation for every method has been covered.

- **Chapter 4**: Experimental work on setting up the source to generate entangled photons and results of various tests (mentioned in the chapter 3) that were performed to characterise the source has been presented.

- **Chapter 5:** We summarize the experimental results and talk on limitations and improvisation of the exisiting experimental setup along with the possible applications of entangled photons in the field of quantum technology.

Part I

Theoretical background

1 Nonlinear optical process

Nonlinear optics is a field of optics that focuses on the study of how light interacts with matter in the presence of high-intensity electromagnetic fields. Nonlinear optical processes are characterized by the generation of new frequencies, as well as the modulation of the amplitude or phase of the incident light. To describe these processes, a set of equations known as nonlinear wave equations are used [15].

In this section, we will delve into the fundamental principles of nonlinear optical processes, including the physical mechanisms that govern them, the mathematical formalism employed to describe them, and a few applications of these processes. This information is crucial for gaining a better understanding of how light behaves in materials and for developing new technologies that rely on nonlinear optical processes.

When light is incident on a dipolar medium then the dipoles start oscillating at the frequency of the light beam. We treat this mechanism to be analogous to the classical simple harmonic oscillator. But when we incident a beam with very high intensity, an anharmonicity is observed in the oscillations of the simple harmonic oscillator. The mathematical representation of the above physical mechanism is :

$$\frac{d^2x}{dt^2} + 2\gamma\frac{dx}{dt} + \omega_0^2 x + \alpha x^2 = F = -\frac{e}{m}E(t) \tag{1}$$

where the first term contributes to the acceleration motion of the oscillator; the second term corresponds to the damping of the oscillation mainly due to non-radiative terms; the third term represents the restoring force of the electron towards its core; the last term is the one that brings anharmonicity in the system. F is the force, e - electronic charge, m - mass of the electron. We can ignore the fourth term when the beam intensity is low. But at high intensity, nonlinearities are introduced leading to many new phenomena like second harmonic wave generation, sum-difference frequency generation, etc.

The polarization that happens inside a medium full of charges can be represented as ,

$$\vec{D} = \epsilon_o \vec{E} + \vec{P} \tag{2}$$

where $\vec{D}$ is the displacement term , $\vec{E}$ is the electric field of the incident light , $\vec{P}$ is the polarization term.

$$\vec{P} = \vec{P_L} + \vec{P_{NL}}$$

where $\vec{P_L}$ depicts the linearly polarized dipoles in the medium and $\vec{P_{NL}}$ corresponds to nonlinearly polarised dipoles in the medium due to high intensity beam.

$$\vec{P_L} = \epsilon_0 \chi^{(1)} \vec{E}$$

$$\vec{P_{NL}} = \epsilon_0 \chi^{(2)} \vec{E^2} + \epsilon_0 \chi^{(3)} \vec{E^3} + ...$$

χ is the nonlinear susceptibility of the medium.

$$\vec{D} = \epsilon_0 \vec{E} + \epsilon_0 \chi^{(1)} \vec{E} + \vec{P_{NL}}$$

$$\vec{D} = \epsilon_0 (1 + \chi^{(1)}) \vec{E} + \vec{P_{NL}}$$

$$\vec{D} = \epsilon \vec{E} + \vec{P_{NL}}$$

On using Maxwell's equations, we can get,

$$\nabla^2 \vec{E} - \mu_0 \epsilon \frac{\partial^2 \vec{E}}{\partial t^2} = \mu_0 \frac{\partial^2 \vec{P_{NL}}}{\partial t^2} \tag{3}$$

Nonlinear optical processes can be broadly classified into two types: second-order and third-order processes. Second-order processes involve the interaction of two photons with a nonlinear material. The physical mechanism that governs this process is known as the second-order nonlinear susceptibility denoted as $\chi^{(2)}$. This quantity relates the induced polarization to the intensity of the applied electric field as :

$$\vec{P_L^2} = \epsilon_0 \chi^{(2)} \vec{E^2}$$

Electro optic effect, second harmonic generation and optical parametric amplification are some of the second order processes.

Third-order nonlinear optical processes involve the interaction of three photons with a nonlinear material. The physical mechanism that governs this process is known as the third-order nonlinear susceptibility denoted as $\chi^{(3)}$. The third-order nonlinear susceptibility is also a tensor, which depends on the crystal symmetry of the material. The polarization is related to the electric field through the third-order nonlinear susceptibility as follows:

$$\vec{P_L^3} = \epsilon_0 \chi^{(3)} \vec{E^3}$$

Third harmonic generation, Optical Kerr effect, Four wave mixing and Stimulated Raman scattering are some of the third order nonlinear processes.

2 Nonlinear optical crystal

The optics of nonlinear crystals is an intriguing area of research that delves into how light behaves when it interacts with materials that possess nonlinear optical properties. Nonlinear crystals have a remarkable capability to alter the frequency, polarization, and phase of light, rendering them invaluable for various applications, including telecommunications, laser technology, and quantum information processing. Having a grasp of the principles of nonlinear optics is critical for advancing current technologies and developing new ones.

There exist two fundamental types of media: isotropic and anisotropic. Isotropic media display a uniform refractive index in all directions, while anisotropic media have refractive indices that rely on both the direction of wave propagation and the polarization state of the incident beam. Nonlinear crystals, in particular, have unique characteristics that depend on the polarization state of the light beam. These beams are classified as either ordinary or extraordinary, with the corresponding refractive indices referred to as the ordinary refractive index or extraordinary refractive index, respectively. The direction where both ordinary and extraordinary refractive indices are equivalent is termed the optic axis of the crystal. Crystals with a single optic axis are known as uniaxial crystals, while those with two optic axes are referred to as biaxial crystals.

When the optic axis of a crystal is aligned with the Z-axis, the principal plane is the area in which the wave vectors **K** and **Z** of a light wave are confined [24]. The ordinary beam, or o-beam, is a light beam whose polarization is perpendicular to the principal plane. In contrast, the ex-

traordinary beam, or e-beam, is polarized within the principal plane. The difference between the refractive indices of ordinary and extraordinary beams is called birefringence. This property is a critical characteristic of anisotropic media and is utilized in a variety of applications in optics and photonics.

$$\Delta n = n_o - n_e$$

where Δn is the birefringence, n_o is the ordinary refractive index and n_e is the extraordinary refractive index. The birefringence has its maximum value in the direction normal to the optic axis and is zero along the optic axis.

In the plane that is perpendicular to the Z-axis, the refractive indices of the ordinary and extraordinary beams are referred to as the principal values of the refractive index, represented by n^o and n^e, respectively [24]. The refractive index of the o-beam is independent of the direction of propagation and is thus represented by a spherical surface with a radius of n_o. In contrast, the refractive index of the e-beam varies with the polar angle (θ), which is the angle between the optic axis **Z** and the wave vector **K**. This variation is due to the anisotropic nature of the crystal and is described mathematically as a function of the angle θ given by the equation,

$$n_e(\theta) = n^o \sqrt{\frac{1+\tan^2\theta}{1+(\frac{n^o}{n^e})^2\tan^2\theta}}$$

And is represented by an ellipsoid with semiaxes n_o and n_e.

If $n_o > n_e$, then it is a negative crystal; if $n_o < n_e$, then it is a positive crystal [Fig :1]

The walk off angle or birefringence ρ can be represented as [Fig :2]:

$$\rho(\theta) = \pm \arctan\left(\frac{n_o}{n_e}\right)^2 \tan\theta \mp \theta$$

where the upper sign refers to a negative crystal and the lower sign to a positive one.

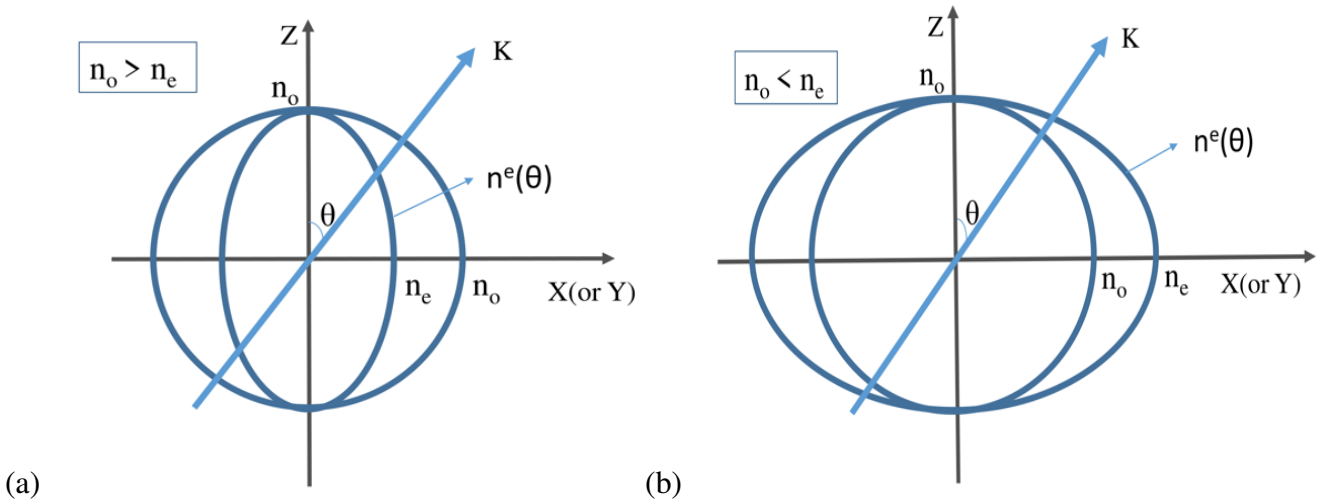

Figure 1: Refractive index dependence on the polar angle (θ) in (a) negative (b) positive uniaxial crystals.

We can use the correlation between ρ and θ to orient uniaxial crystals. After the incident beam passes through the crystal they are separated by δ at the output surface of the crystal which is given by:

$$\delta = L \tan \rho$$

Knowing the crystal cut angle (θ_c) which is between the optic axis **Z** and the normal to the crystal surface is essential for designing and optimizing nonlinear optical processes and for controlling the polarization of the output light [Fig :3]. By choosing the appropriate crystal cut angle, it is possible to achieve different polarization properties of the output light, such as linear polarization, circular polarization, or elliptical polarization which is given by:

$$\theta_c = \arctan\left(\frac{|n_o^2 - n_e^2|L}{2\delta n_o^2} \pm \left(\frac{|(n_o^2 - n_e^2)^2 L^2|}{|4\delta^2 n_o^4|} - \frac{n_o^2}{n_e^2}\right)^{1/2}\right)$$

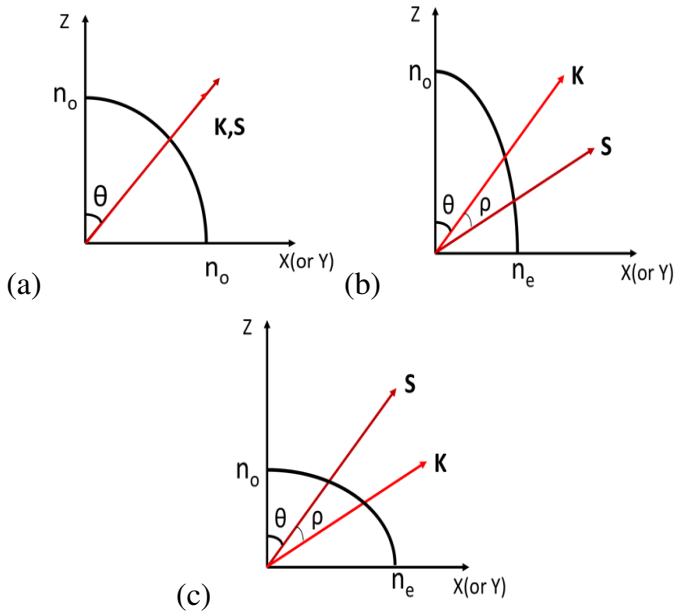

Figure 2: Transmission of the wave vector (**K**) and beam vector (**S**) in an (a) isotropic medium and anisotropic (b) negative and (c) positive uniaxial crystals (ρ is the birefringence angle).

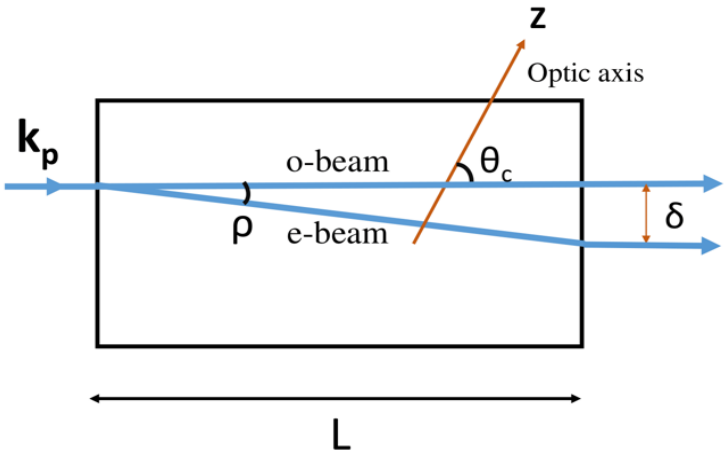

Figure 3: Schematic representation of the uniaxial crystal with cut angle θ_c.

3 Spontaneous parametric down conversion (SPDC)

Entangled photon pairs can be generated using various methods such as semiconductor quantum dots, atomic ensembles, microresonators, and parametric amplifiers. Semiconductor quantum dots emit entangled photons when excited by a laser, while atomic ensembles like rubidium vapor can emit entangled photon pairs through collective excitation. Microresonators, such as whispering gallery resonators, can generate entangled photons through spontaneous four-wave mixing, while

parametric amplifiers amplify vacuum field fluctuations to produce entangled photon pairs. Each of these methods has unique advantages and disadvantages and can be optimized for specific applications. We shall be specifically looking at the generation of entangled photons using spontaneous parametric down conversion process.

When a beam of photons interacts with a nonlinear crystal, it undergoes a second-order optical phenomenon known as spontaneous parametric down-conversion (SPDC) [26, 25] [Fig:4]. The down-conversion process occurs when a photon, called the pump photon, interacts with a nonlinear crystal and spontaneously splits into two lower-energy photons, known as the idler and signal photons. This process is considered spontaneous, as it occurs without any external frequency input. The phenomenon is referred to as parametric because it depends on the order of the electric field and creates a phase relationship between the input and output fields. Therefore, the down-conversion process is a result of the parametric interaction between the pump photon and the nonlinear crystal, leading to the spontaneous creation of two photons.

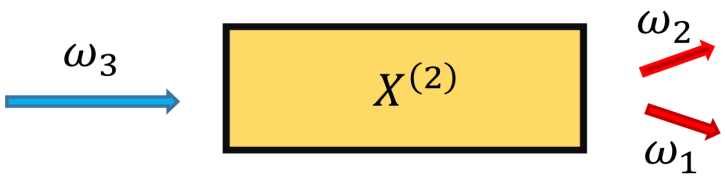

Figure 4: Schematic representation of SPDC process. Pump photon (ω_3) falls on a nonlinear crystal with susceptibility χ^2 and gets converted to signal (ω_2) and idler (ω_1) photons.

This conversion process happens in accordance with the laws of conservation of energy and momentum. The conservation of energy says that the energy of the incident photons must be equal to the energy of down converted photons (Fig:5). So,

$$\hbar\omega_3 = \hbar\omega_2 + \hbar\omega_1$$

$$\omega_3 = \omega_2 + \omega_1$$

The conservation of momentum says that the momentum of pump photon must be equal to momenta of signal and idler photons (Fig:6).

$$\boldsymbol{k_3 = k_2 + k_1}$$

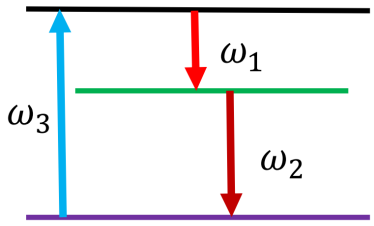

Figure 5: Schematic representation of energy conservation in SPDC process.

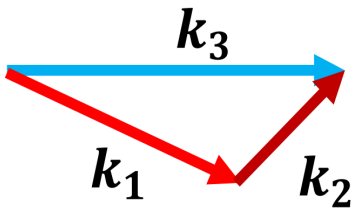

Figure 6: Schematic representation of momentum conservation in SPDC process.

The mechanism that lies behind the down conversion process is **Optical rectification**. When a nonlinear crystal is incident with a photon of frequency ω at very high intensity then there is a generation of quasi-DC polarization which is responsible for resizing the dipoles and hence the frequency with which they oscillate. This mechanism is seen only when we incident the nonlinear crystal with high intensity beam (Fig:3).

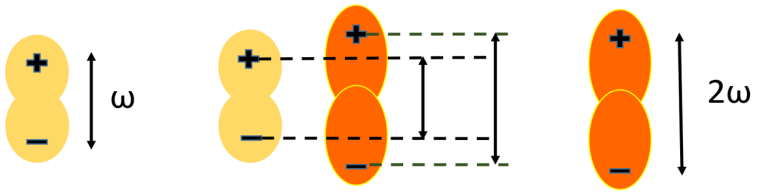

Figure 7: Pictorial representation of Optical rectification from $\omega \rightarrow 2\omega$.

In this SPDC process, we are shining pump photons with electric field $\boldsymbol{E}^{(\omega_p)}$ having amplitude E_p , wave vector $\boldsymbol{k_p}$ with frequency ω_p along $\mathbf{z}$ direction. Signal and idler photons having electric field $\boldsymbol{E}^{(\omega_s)}$, $\boldsymbol{E}^{(\omega_i)}$; amplitude E_s, E_i ; wave vector $\boldsymbol{k_s}, \boldsymbol{k_i}$ of frequency ω_s, ω_i respectively are generated.

So the expressions for the fields are:

$$\boldsymbol{E}^{(\omega_p)} = \frac{1}{2}[E_p e^{i(k_p z - \omega_p t)} + c.c] \tag{4}$$

$$\boldsymbol{E}^{(\omega_s)} = \frac{1}{2}[E_s e^{i(k_s z - \omega_s t)} + c.c]$$

$$\boldsymbol{E}^{(\omega_i)} = \frac{1}{2}[E_i e^{i(k_i z - \omega_i t)} + c.c]$$

Hence the total electric field **E** is:

$$\boldsymbol{E} = \boldsymbol{E}^{(\omega_p)} + \boldsymbol{E}^{(\omega_s)} + \boldsymbol{E}^{(\omega_i)}$$

$$\boldsymbol{P_{NL}} = 2d\epsilon_0 E^2 = 2d\epsilon_0[\boldsymbol{E}^{(\omega_p)} + \boldsymbol{E}^{(\omega_s)} + \boldsymbol{E}^{(\omega_i)}]^2$$

where $d = \frac{1}{2\chi^{(2)}}$ is a complex but well-known parameter that depends on the material's strength, nonlinearity, and geometrical variables, all of which are characteristics of the material.

Nonlinear polarization terms that are produced in the medium are :

$$\boldsymbol{P}_{\boldsymbol{NL}}^{(\omega_p)} = \frac{1}{2} d\epsilon_0 [2E_s E_i e^{(k_s + k_i)z - \omega_p t} + c.c] \tag{5}$$

$$\boldsymbol{P}_{\boldsymbol{NL}}^{(\omega_s)} = \frac{1}{2} d\epsilon_0 [2E_p E_i^* e^{(k_p - k_i)z - \omega_s t} + c.c]$$

$$\boldsymbol{P}_{\boldsymbol{NL}}^{(\omega_i)} = \frac{1}{2} d\epsilon_0 [2E_s^* E_p e^{(k_p - k_s)z - \omega_i t} + c.c]$$

On substituting equations 4 and 5 into Maxwell's equation (eq.3) , we get wave equation for ω_p wave:

$$\nabla^2 \vec{E^{\omega_p}} - \mu_0 \epsilon \frac{\partial^2 \vec{E^{\omega_p}}}{\partial t^2} = \mu_0 \frac{\partial^2 \vec{P_{NL}^{(\omega_p)}}}{\partial t^2} \tag{6}$$

The LHS becomes,

$$\nabla^2 \vec{E^{\omega_p}} = \frac{1}{2}[\frac{\partial^2 E_p}{\partial z^2} + 2ik_p \frac{\partial E_p}{\partial z} - k_p^2 E_p] e^{i(k_p z - \omega_p t)} + c.c$$

Now using slowly varying approximation where E_p varies slowly , we can neglect

$$|\frac{\partial^2 E_p}{\partial z^2}| << |\frac{\partial E_p}{\partial z}|$$

So,

$$\nabla^2 \vec{E^{\omega_p}} \approx \frac{1}{2}[2ik_p \frac{\partial E_p}{\partial z} - k_p^2 E_p] e^{i(k_p z - \omega_p t)} + c.c]$$

Substitute eq.5 to RHS of eq.6, we get,

$$\frac{\partial^2 \vec{P}_{NL}^{(\omega_p)}}{\partial t^2} = -\frac{2\omega_p^2}{2}\epsilon_0 d E_s E_i e^{i[(k_s+k_i)z-\omega_p t]} + c.c$$

Now eq.6 becomes,

$$\left[2ik_p\frac{\partial E_p}{\partial z} - k_p^2 E_p - \mu_0\epsilon(-\omega_p^2)E_p\right]e^{ik_p z} = \mu_0\epsilon_0 d E_s E_i(-2\omega_p^2)e^{i(k_s+k_i)z}$$

$$k_p^2 = \left(\frac{\omega_p}{c}\right)^2 n_p^2 = \omega_p^2\mu_0\epsilon_0\epsilon_r = \omega_p^2\mu_0\epsilon$$

where n_p is the refractive index seen by pump photon, c is the speed of light.

$$2ik_p\frac{\partial E_p}{\partial z} = \mu_0\epsilon_0 d E_s E_i(-2\omega_p^2)e^{-i(k_p-k_i-k_s)z}$$

Take $\Delta\boldsymbol{k} = \boldsymbol{k_p} - \boldsymbol{k_s} - \boldsymbol{k_i}$. So,

$$\frac{dE_p}{dz} = i\frac{d\omega_p^2}{k_p c^2}E_s E_i e^{-i\Delta k z} \tag{7}$$

$$\frac{dE_p}{dz} = i\frac{d\omega_p}{n_p c}E_s E_i e^{-i\Delta k z} \tag{8}$$

In the way we have derived eq.8, we can also derive evolution equations for electric field amplitudes of signal and idler photons. So the evolution equations of pump, signal and idler waves are:

$$\frac{dE_p}{dz} = i\frac{d\omega_p}{n_p c}E_s E_i e^{-i\Delta k z} \tag{9}$$

$$\frac{dE_s}{dz} = i\frac{d\omega_s}{n_p c}E_p E_i^* e^{-i\Delta k z} \tag{10}$$

$$\frac{dE_i}{dz} = i\frac{d\omega_i}{n_p c}E_p E_s^* e^{-i\Delta k z} \tag{11}$$

Now let's use the above three equations to show that energy is conserved in this process.

We know that Power = Intensity x Area. On using this formula (for pump photons) we get,

$$P_p(z) = I_p(z)A = \frac{1}{2}\epsilon_0 c n_p |E_P(z)|^2 A \tag{12}$$

where $P_p(z)$ is the power of the pump photon incident on the crystal on an area A with intensity $I_p(z)$. On differentiating the above equation with respect to z, we get,

$$\frac{dP_p(z)}{dz} = \frac{1}{2}\epsilon_0 c n_p A \left[E_p^* \frac{dE_P}{dz} + E_p \frac{dE_p^*}{dz} \right]$$

$$\frac{dP_p(z)}{dz} = \frac{1}{2}\epsilon_0 c n_p A \left[E_p^* i k_p E_s E_i e^{-i\Delta k z} - E_p i k_p E_s^* E_i^* e^{i\Delta k z} \right]$$

$$\frac{dP_p(z)}{dz} = \frac{1}{2}\epsilon_0 c n_p A i k_p \left[E_p^* E_s E_i e^{-i\Delta k z} - E_p E_s^* E_i^* e^{i\Delta k z} \right] \tag{13}$$

$$\frac{dP_p(z)}{dz} = \frac{i}{2}\epsilon_0 d\omega_p A \left[E_p^* E_s E_i e^{-i\Delta k z} - E_p E_s^* E_i^* e^{i\Delta k z} \right] \tag{14}$$

Similarly,

$$\frac{dP_s(z)}{dz} = \frac{i}{2}\epsilon_0 d\omega_s A \left[E_p E_s^* E_i^* e^{i\Delta k z} - E_p^* E_s E_i e^{-i\Delta k z} \right] \tag{15}$$

$$\frac{dP_i(z)}{dz} = \frac{i}{2}\epsilon_0 d\omega_i A \left[E_s^* E_p E_i^* e^{i\Delta k z} - E_s E_p^* E_i e^{-i\Delta k z} \right] \tag{16}$$

where $P_s(z), P_i(z)$ represent the power of signal and idler photons.

From the above last three equations, we can get,

$$-\frac{1}{\omega_P}\frac{dP_p}{dz} = \frac{1}{\omega_s}\frac{dP_s}{dz} = \frac{1}{\omega_i}\frac{dP_i}{dz} \tag{17}$$

which is the famous Manley-Rowe relation from which we can show that the total power is conserved in the SPDC process i.e.

$$-\frac{1}{\omega_P}\frac{dP_p}{dz} = \frac{1}{\omega_s}\frac{dP_s}{dz} = \frac{1}{\omega_i}\frac{dP_i}{dz} = \Gamma \tag{18}$$

(Γ is a constant)

$$\frac{dP_p}{dz} + \frac{dP_s}{dz} + \frac{dP_i}{dz} = \Gamma(-\omega_p + \omega_s + \omega_i)$$

$$P = P_p + P_s + P_i$$

$$\frac{dP}{dz} = \Gamma \times 0 = 0; \omega_p = \omega_s + \omega_i \tag{19}$$

So total power P is conserved.

Now for a degenrate parametric down conversion, say, from $2\omega \rightarrow \omega + \omega$, for $\Delta k = 0$,

$$\frac{dE_p}{dz} = i\frac{d\omega}{n_1 c} E_p E_s^* \tag{20}$$

$$\frac{dE_p}{dz} = i\frac{d\omega}{n_2 c} E_s E_i \tag{21}$$

Under no depletion approximation, $E_p = constant$ (pump photon) and also $E_s(0) = 0$.(down converted photon)

Again on differentiating Eq.20, we get,

$$\frac{d^2E_s}{dz^2} = i\frac{d\omega}{n_1 c} E_p \left(\frac{dE_s^*}{dz}\right)$$

On substituting E_s,

$$\frac{d^2E_s}{dz^2} = i\frac{d\omega}{n_1 c} E_p \left(-i\frac{d\omega}{n_1 c} E_p^* E_s\right)$$

$$\frac{d^2E_1}{dz^2} = \left(\frac{d\omega}{n_1 c}\right)^2 |E_2|^2 E_1 \tag{22}$$

$$\Upsilon^2 = \left(\frac{d\omega}{n_1 c}\right)^2 |E_p|^2$$

$$\frac{d^2E_s}{dz^2} = \Upsilon^2 E_s \tag{23}$$

$$E_s(z) = Asinh(\Upsilon z) + Bcosh(\Upsilon z) \tag{24}$$

Now at z = 0, $E_s(z = 0) = 0$; that means B = 0 implying that at z = 0, only pump photons are just incident on the crystal and conversion process has not begun at.

So,

$$E_s(z) = Asinh(\Upsilon z)$$

Again,

$$\left[\frac{dE_s}{dz}\right]_{z=0} = i\frac{\omega d}{n_1 c}E_p(0)E_s^*(0) = 0$$

$$\left[\frac{dE_s}{dz}\right]_{z=0} = A\Upsilon cosh(\Upsilon z)|_{z=0} = A\Upsilon = 0 \tag{25}$$

Here $\Upsilon \neq 0$, so A=0 which means $E_s(z) = 0$, so classically there will be no frequency down conversion where there is no input field containing ω frequency. That is, without any quantum noise we cannot generate any sub-harmonics. We can see that classical optics won't allow for the SPDC process to exist. So SPDC is purely a quantum mechanical process.

3.0.1 Birefringence Phase Matching

Birefringence refers to the characteristic of certain materials that results in their refractive index being dependent on the polarization and direction of light propagation. Such materials are termed optically anisotropic and are known as birefringent.

For a conversion process from $\omega_p \rightarrow \omega_s + \omega_i$,
The phase matching condition is $\Delta\boldsymbol{k} = 0 \Longrightarrow \boldsymbol{k_p - k_s - k_i} = 0$
W.K.T,

$$\boldsymbol{k_{p,s,i}} = \omega_{p,s,i} n_{p,s,i}/c$$

where $\boldsymbol{k_{p,s,i}}$ are wave vectors of the pump, signal and idler photons; $n_{p,s,i}$ are the refractive indices of the medium seen by pump, signal and idler photon; $\omega_{p,s,i}$ are the frequency of the pump, signal and idler photons; c is the speed of light. Hence we get phase matching condition to be,

$$n_{p\sigma}\omega_p - n_{s\sigma}\omega_s = \frac{\omega_p}{\omega_i}\left[n_{i\sigma}\omega_i - n_{s\sigma}\omega_s\right]$$

3.0.2 Types of phase matching in uniaxial crystal

When the pump, signal, and idler photons have the same polarization, it is known as **Type-0** phase matching. **Type-1** phase matching occurs when the signal and idler have the same polarization but are orthogonal to the pump polarization. **Type-2** phase matching occurs when the signal and idler have orthogonal polarizations.

Collinear phase matching occurs when the optical path of the pump, idler, and signal are all in the same direction. On the other hand, **non-collinear phase matching** occurs when the signal and idler photons propagate in directions that are not collinear with the pump photon direction.

From momentum and energy conservation, we can derive

$$n_{p\sigma}\omega_p - n_{s\sigma}\omega_s = \frac{\omega_p}{\omega_i}\left[n_{i\sigma}\omega_i - n_{s\sigma}\omega_s\right] \tag{26}$$

σ index represents the polarization state of the photons as ordinary or extraordinary. n_σ represents the ordinary or extraordinary refractive index.

But, due to normal dispersion, w.k.t ,

$$n_{p\sigma}(\omega_p) > n_{s\sigma}(\omega_s) \geq n_{i\sigma}(\omega_i). \tag{27}$$

Now we shall try which polarization states of the photons can phase match.

Case 1:$e \longrightarrow e + e$

Pump, signal and idler photons are extraordinarily polarized. For this case, Eq.26 becomes:

$$n_{pe}\omega_p - n_{se}\omega_s = \frac{\omega_p}{\omega_i}\left[n_{ie}\omega_i - n_{se}\omega_s\right]$$

and due to eqn.27, $n_{pe}(\omega_p) > n_{se}(\omega_s) \geq n_{ie}(\omega_i)$. Hence the conditions necessary for phase matching are not met by these particular polarization states. Therefore, phase matching cannot occur for these states of polarization.

Case 2: $o \longrightarrow o + o$

Pump, signal and idler photons are ordinarily polarized. For this case, Eq.26 becomes:

$$n_{po}\omega_p - n_{so}\omega_s = \frac{\omega_p}{\omega_i}\left[n_{io}\omega_i - n_{so}\omega_s\right]$$

and due to eqn.27, $n_{po}(\omega_p) > n_{so}(\omega_s) \geq n_{io}(\omega_i)$. Hence the conditions necessary for phase matching are not met by these particular polarization states. Therefore, phase matching cannot occur for these states of polarization.

Case 3: $e \longrightarrow o + o$

Pump photons are extraordinarily polarized whereas signal and idler photons are ordinarily polarized. For this case, Eq.26 becomes:

$$n_{pe}\omega_p - n_{so}\omega_s = \frac{\omega_p}{\omega_i}\left[n_{io}\omega_i - n_{so}\omega_s\right]$$

As $\omega_s \geq \omega_i$, the RHS of the equation is negative. For LHS to be negative , $n_e < n_o$, implies that the crystal has to be negative. Negative uniaxial crystals, such as Beta Barium Borate (BBO), have the ability to fulfill the conditions necessary for phase matching. Therefore, it is possible for phase matching to occur in these types of crystals.

Case 4: $o \longrightarrow e + e$

Pump photons are ordinarily polarized whereas signal and idler photons are extraordinarily polarized. For this case, Eq.26 becomes:

$$n_{po}\omega_p - n_{se}\omega_s = \frac{\omega_p}{\omega_i}\left[n_{ie}\omega_i - n_{se}\omega_s\right]$$

As $\omega_s \geq \omega_i$, the RHS of the equation is negative. For LHS to be negative, $n_e > n_o$, implies that the crystal has to be positive. So positive uniaxial crystals can satisfy the phase matching condition.

Case 5: $e \longrightarrow o + e$

Pump photons are extraordinarily polarized whereas signal is ordinarily and idler photons are extraordinarily polarized. For this case, Eq.26 becomes:

$$n_{pe}\omega_p - n_{so}\omega_s = \frac{\omega_p}{\omega_i}\left[n_{ie}\omega_i - n_{so}\omega_s\right]$$

Suppose we consider a degenerate source of SPDC, and assume linear dispersion relation for both extraordinary and ordinary polarizations. So, $n_{pe}(2\omega_s) \approx 2n_{pe}(\omega_s)$. Now, substituting $n_{pe}(\omega_s) = n_{ie}(\omega_s) = n_e(\omega_s); n_{so}(\omega_s) = n_o(\omega_s)$,

We write the above equation as,

$$3n_e(\omega_s) \approx n_o(\omega_s).$$

But this equation exists if $n_e < n_o$. So only negative uniaxial crystals can phase match for these polarization states.

Case 6: $e \longrightarrow e + o$

Pump photons are extraordinarily polarized whereas signal is extraordinarily and idler photons are ordinarily polarized. For this case, Eq.26 becomes:

$$n_{pe}\omega_p - n_{se}\omega_s = \frac{\omega_p}{\omega_i}\left[n_{io}\omega_i - n_{se}\omega_s\right]$$

Considering all the assumptions from the case 5, and

$$3n_e(\omega_s) \approx n_o(\omega_i).$$

The above equation is true only if $n_e < n_o$. So only negative uniaxial crystals can phase match for these polarization states.

Case 7: $o \longrightarrow e + o$

Pump photons are ordinarily polarized whereas signal is extraordinarily and idler photons are ordinarily polarized. For this case, Eq. 26 becomes:

$$n_{po}\omega_p - n_{se}\omega_s = \frac{\omega_p}{\omega_i}\left[n_{io}\omega_i - n_{se}\omega_s\right]$$

Considering all the assumptions from the case 5, and

$$3n_o(\omega_s) \approx n_e(\omega_s).$$

The above equation is true only if $n_o < n_e$. So only positive uniaxial crystals can phase match for these polarization states.

Case 8: $o \longrightarrow o + e$

Pump photons are ordinarily polarized whereas signal is extraordinarily and idler photons are ordinarily polarized. For this case, Eq.26 becomes:

$$n_{po}\omega_p - n_{so}\omega_s = \frac{\omega_p}{\omega_i}\left[n_{ie}\omega_i - n_{so}\omega_s\right]$$

Considering all the assumptions from the case 5, and

$$3n_o(\omega_s) \approx n_e(\omega_s).$$

The above equation is true only if $n_o < n_e$. So only positive uniaxial crystals can phase match for these polarization states.

Type	Positive uniaxial	Negative uniaxial
Type-1	o → e + e	e → o + o
Type-2	o → o + e	e → e + o
Type-2	o → e + o	e → o + e

Table 1: Summary of polarization states that allow phase matching between pump , signal and idler photons.

3.0.3 Quasi Phase Matching (QPM)

In a nonlinear media, quasi-phase matching is a technique used to successfully transmit energy from the pump frequency to the signal and idler frequencies. This is accomplished by forming a periodic structure inside the medium that allows energy to be transferred when the phase difference between the pump and down-converted photons is equal to or less than 180° [27]. If the phase difference surpasses 180°, the energy will flow back from the down-converted photons to the pump photons. The medium's coherence length is the space between which the sum of down-converted frequencies and the phase of the pump is exactly 180° apart. The crystal axes are flipped at each coherence length, allowing energy to flow from the pump to the down-converted photons.

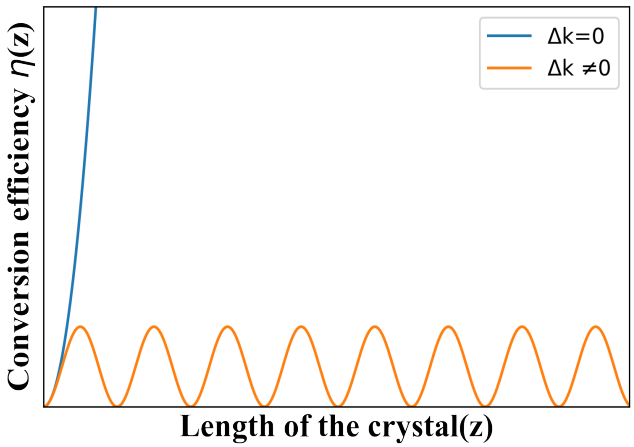

Figure 8: Graph of conversion efficiency vs length of the crystal.

The mechanism is as follows:

Look at the figure :8 which depicts the conversion efficiency ($\eta(z)$) along the length of the crystal (z). We can seen that the conversion efficiency from pump photon to down converted photons is sinusoidal when $\Delta \boldsymbol{k} \neq 0$. To achieve $\Delta \boldsymbol{k} = 0$, we can use the QPM technique where the crystals are periodically poled such that the wave vector of the periodic structure satisfies the phase matching condition so that momentum is conserved.

Periodic poling is a technique used to produce a periodic reversal in the domain orientation of a nonlinear crystal, resulting in a change in the sign of the nonlinear coefficient ($d(z)$). This process enables the efficient conversion of pump photons to down-converted photons within the coherence length, where the nonlinear coefficient is positive. However, beyond this length, conversion from

down-converted photons to pump photons reduces the conversion efficiency. To overcome this loss, periodic poling reverses the nonlinear coefficient of the material, resulting in increased conversion efficiency.

If $\boldsymbol{K_Q}$ is the wavevector of the material, Λ is the wavelength of the sinusoidally varying nonlinear coefficient, d(z) where d(z) = $d_0 sin(\boldsymbol{K_Q} z)$, then

$$\boldsymbol{K_Q} = \frac{2\pi}{\Lambda}$$

For phase matching,

$$\boldsymbol{K_Q} = \boldsymbol{\Delta k} = \frac{2\pi}{\Lambda}$$

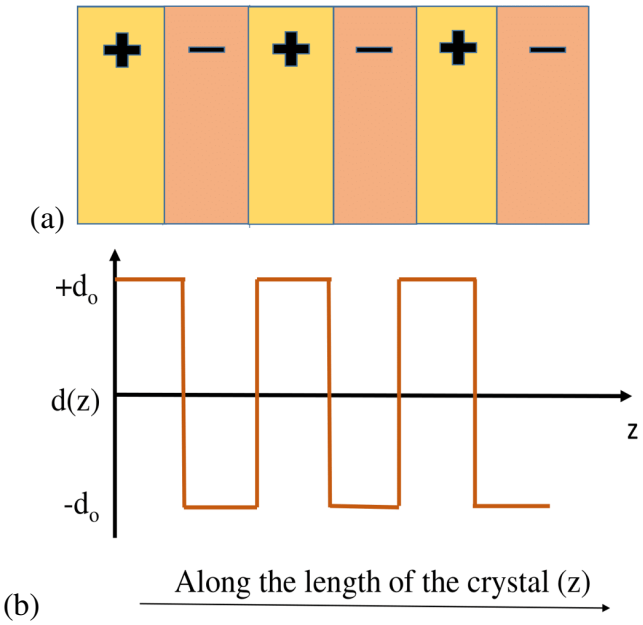

Figure 9: Periodically poled QPM structure. (a) At every coherence length, the domain of the crystal is inversed. (b) Nonlinear coefficient along the length of the crystal.

Then the coherence length L_c can be calculated as:

$$L_c = \frac{\pi}{\boldsymbol{\Delta k}} = \frac{\Lambda}{2}$$

So if we make sure that the wavelength of the sinusoidally varying nonlinear coefficient d(z) is twice the coherence length then phase matching conditions can be met [Fig :9].

So we have discussed here only the classical aspect of SPDC and saw that it is a mechanism where photons of higher energy get converted to photons of lower energy on passing through a nonlinear medium. This process is in accordance with conservation of energy and momentum and they are met through phase matching condition, $\Delta \boldsymbol{k} = 0$ where methods like Birefringence phase matching and Quasi phase matching conditions have been used to meet this criterion.

Part II

Schemes for generating entangled photons

4 Entanglement

In this section, let us understand how polarisation-entangled photon pairs can be produced. Consider two SPDC sources (Imagine these two sources as two harmonic oscillators inside the same nonlinear crystal which are spatially separated) which emit orthogonally polarised photon pairs in a state $\mid H,1\rangle_s \mid V,1\rangle_i and \mid V,2\rangle_s \mid H,2\rangle_i$ where the labels (1, 2) denote any spatial, spectral or temporal features from the respective sources 1 and 2 [4]. Now, we clearly know the polarization state of the photons and it's source. This introduces distinguishability between the photons. The observed state here will just be product states.

Mathematically, entanglement of two states has been defined as,

$$|\Psi\rangle_{AB} \neq |\Psi\rangle_A \otimes |\Psi\rangle_B$$

where $|\Psi\rangle_A$ belongs to Hilbert space A and $|\Psi\rangle_B$ belongs to Hilbert space B. Implies we cannot write the entangled state as tensor product of two independent states.
If we try to express the joint projective polarization measurement of the signal and idler photons in a superposition basis,

$$\mid \phi_{s,i}\rangle = \sqrt{1/2}(\mid H\rangle_{s,i} + e^{i\phi_{s,i}} \mid V\rangle_{s,i})$$

Then probability for coincidence detection is given by,

$$p(\phi_s,\phi_i) = \mid \langle \phi_i \mid \langle \phi_s \mid \Psi\rangle \mid^2 = \frac{1}{2}(1 + Re(e^{i(\phi_s-\phi_i)}\langle 1|_i\langle 1|_s|2\rangle_s \mid 2\rangle_i)) \tag{28}$$

If we can distinguish the photon pairs emitted from the two sources, that is, $\langle 1|_i\langle 1|_s|2\rangle_s \mid 2\rangle_i$ where s and i corresponding to orthogonal states, then, the phase factor vanishes; hence we cannot observe the characteristic non-local coherence of a polarization-entangled state. So we need to remove the information regarding their spatial features. There are few methods through which we can remove spatial distinguishability. For example, by interferometry, geometry, birefringence and momentum selection.

- In the Interferometric method, amplitude interference of down-converted beams is accom-

plished by employing either a polarizing beam splitter or a normal beam splitter. Specifically, the two orthogonal states of photons are made to interfere with a beam splitter. After post-selection, which occurs at the output port of the beam splitter, entangled photons are obtained.

- Entangled photons can also be obtained by superposing two pairs of orthogonally polarized photons on a polarizing beam splitter, followed by post-selection. However, any residual spatially distinguishable photons can be eliminated by implementing spatial filters, such as the use of single mode fibers. It should be noted that this filtering process reduces the efficiency of the source by at least 50%.

- Another approach to obtain entangled photons involves designing the nonlinear crystal to ensure that the down-converted signal and idler cones overlap, using the appropriate phase matching conditions, such as type-0, type-1 or type-2, to establish indistinguishability in both spectral and spatial modes.

- The momentum selection method, typically employed by type-2 phase matching crystals, involves selecting specific momentum components to achieve indistinguishability between down-converted photons. For instance, one can select photons from the region of the intersection of two cones in type-2 crystals.

Once spatial distinguishability has been eliminated, it becomes evident that probability is dependent on the phase factor. Maximum coincidence detection is achieved when the phases of both signal and idler are identical, resulting in maximally entangled photons. These maximally-entangled states are referred to as Bell states. Thus, it is crucial to minimize phase dependence in order to achieve high-quality entangled photons. Post-compensation and pre-compensation methods are two techniques that can be used to remove the dependence of the phase factor on the pump wavelength. Post-compensation reduces the relative phase as a function of pump wavelength only, which can be achieved using YVO_4 crystals.

$$\varphi(\lambda_p, \lambda_s, \lambda_i) \rightarrow \varphi(\lambda_p)$$

On the other hand, pre-compensation methods remove the dependence of the pump wavelength in the phase factor so that it becomes a constant $[\varphi(\lambda_p) \rightarrow \varphi_c]$. Wave plates can be used to eliminate the constant phase factor, thereby producing Bell states.

The down-converted wavelengths produced in SPDC cover a broad range, and passing them through various optical components such as dispersive mediums can result in spectral distinguishability due to wavelength-dependent phase. To remove this phase dependence and improve the quality of entanglement, compensation crystals such as YVO_4 can be employed.

Temporal distinguishability, on the other hand, can be eliminated using waveplates and nonlinear crystals that are half as big as the main crystals used to down convert photons. The distinguishing characteristics of the temporal wave function occur in the picosecond period, while the detector's timing resolution is on the order of nanosecond. Therefore, the experimental setup can aid in the creation of indistinguishability.

We can see that the down converted photons are forced to become entangled in polarisation degree of freedom. Photons from SPDC source are inherently entangled in time-energy, position-momentum, orbital angular momentum degrees of freedom. But to measure these entangled photons we need sophisticated setups. For example, for time-energy entangled photons we would need an interferometer based measurement. So it requires an interferometric alignment. Position-momentum entangled photons are restricted by short distances because on coupling the photons to a single mode fiber the information is lost whereas orbital angular momentum requires complex spatial light modulators for making measurements.

5 Types of schemes to generate entangled photons

5.1 Single crystal, single pass configuration

5.1.1 Type-2 Bulk crystals

On incident a pump beam perpendicular to a type-2 single bulk crystal we get two cones of signal and idler beam respectively [16]. One cone is ordinarily polarized where as the other cone is extraordinarily polarized. The two cones are separated because of the walk-off angle experienced by the extraordinary beam. We need to incident the pump beam in such a way that the two cones intersect and at the point of intersection we have "indistinguishable" polarisation-entangled photons [Fig: 10]. The reason for extracting photons at the point of intersection is that it enables indistinguishability which is the main criterion of entangled photons. Choosing photons from any other points will give us product states but not entangled photons.

The entangled state for this configuration can be mathematically represented as,

$$|H\rangle_1 |V\rangle_2 \pm e^{i\varphi} |V\rangle_1 |H\rangle_2$$

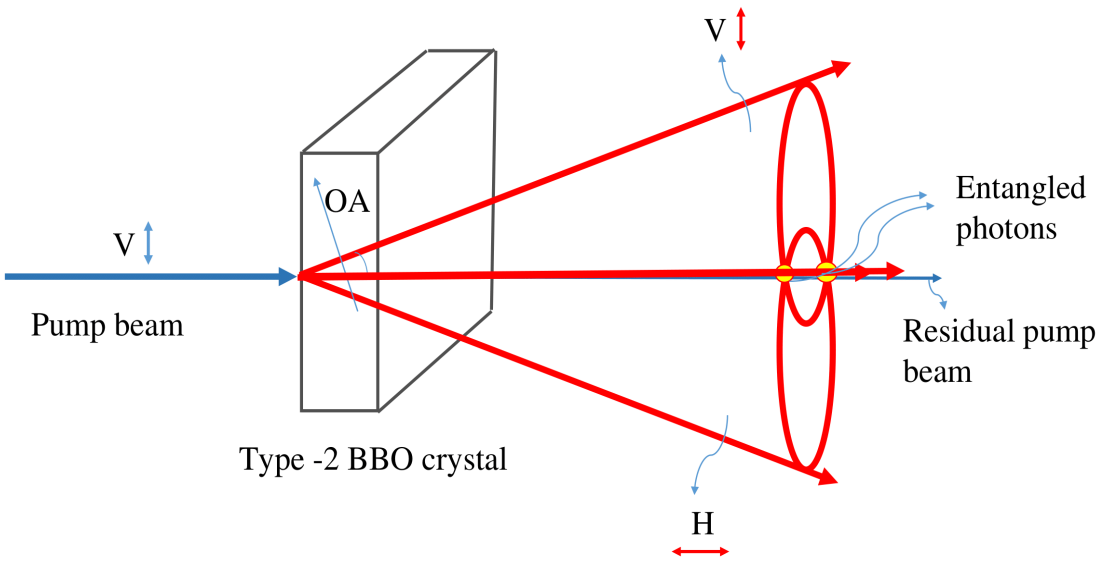

Figure 10: Schematic representation of type-II SPDC photon source.

5.2 Double crystal, single pass configuration

Non-collinear configurations

5.2.1 Crossed type-1 crystals

We know that in type-1, down converted photos have the same polarization. Hence there is no birefringence and the two cones overlap with each other. We can make use of two type-1 crystals and orient their optic axis orthogonal to each other. For this orientation, we need to incident diagonally polarized pump beam [Fig :11]. One crystal converts all horizontally polarized pump photons whereas another crystal converts vertically polarised photons [29]. Since there is no walk-off between the two beams, we can orient the crystal in such a way that the cones from both crystals overlap perfectly and hence indistinguishability is established everywhere. Hence type-1 sources are more efficient than the previously mentioned scheme.

Mathematically we can represent the entangled state as,

$$|H\rangle_1 |H\rangle_2 \pm e^{i\varphi} |V\rangle_1 |V\rangle_2$$

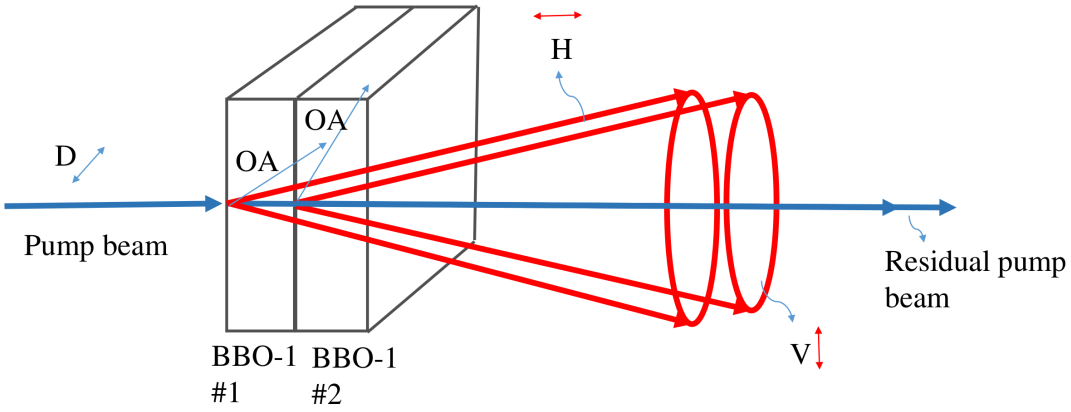

Figure 11: Schematic representation of crossed type-1 SPDC photon source.

5.2.2 Flipped type-2 crystals:

We can use two type-2 crystals and orient the optic axis of one crystal at 180^0 with respect to another crystal [Fig :12]. Each crystal produces a set of rings whose polarization orientation is also flipped by 180^0. Indistinguishability is established in any diametric pairs across either ring [30].

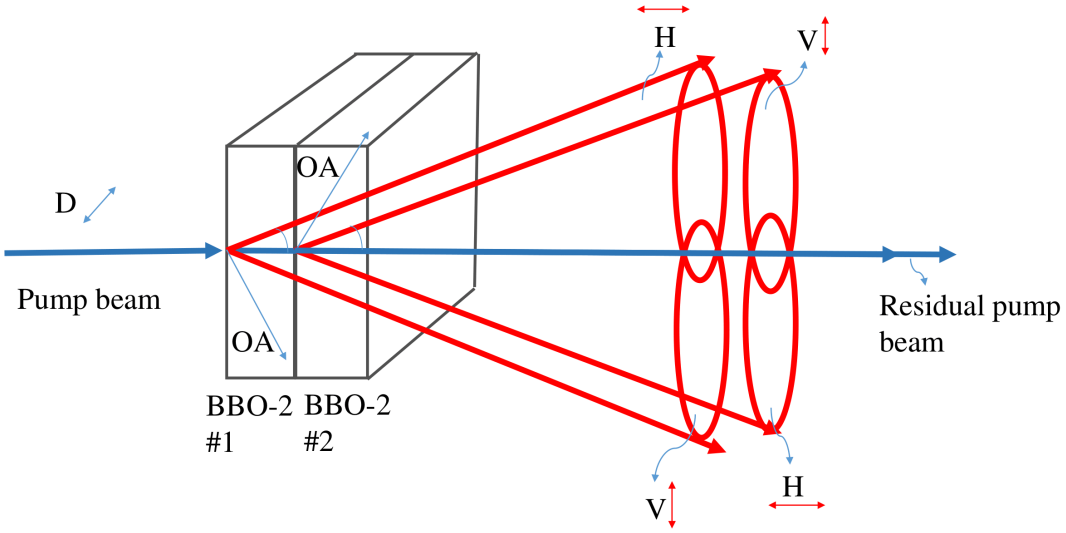

Figure 12: Schematic representation of SPDC in flipped bulk type-2 crystal.

5.2.3 Crossed type-2 crystals:

Using two type-2 bulk crystals, we can orient their optic axis orthogonal to each other. A diagonally polarized pump beam can excite both crystals giving a set of down converted rings that are also orthogonal to each other [31]. From this configuration, we get 12 intersection points for procuring indistinguishable entangled photons.

The highlighted points 5, 6, 7, and 8 from the figure :13 are the standard Bell states, where pair (5, 6) originates from crystal 1 and pair (7, 8) originates from crystal 2. Points 1, 2, 3, and 4 are the result of the product of two bell states generated simultaneously using photons from crystals 1 and 2. Points (9, 11) and (10, 12) are VV and HH states generated simultaneously by photons from crystals 1 and 2 respectively.

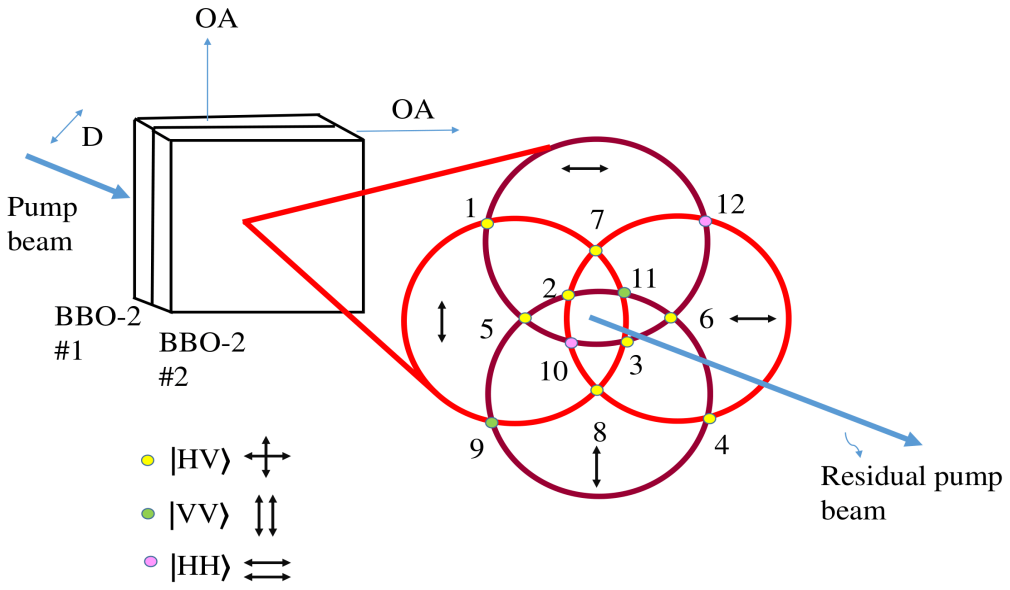

Figure 13: Schematic representation of crossed type-2 bulk crystals.

5.2.4 Sandwiched double crystals

We can also use two type-2 crystals whose optic axis are parallel to each other but are sandwiched by a HWP [32] [Fig:14]. We can pump a vertically polarized beam instead of diagonal. First the crystal converts a horizontal pump beam to a horizontally polarised ordinary beam and a vertically polarised extraordinary beam. The HWP converts the vertical pump beam into a horizontal pump beam and incidents it on the second crystal. The second crystal converts the vertical beam to a vertically polarized ordinary beam and a horizontally polarised extraordinary beam.

Collinear schemes

5.2.5 Position correlations

We can also force position correlated photons in SPDC into polarization entanglement [4] [Fig :15]. For example, we can use a type-0 PPKTP crystal and manipulate the polarization state of only half of its down converted photons using a segmented HWP and later we can establish spatial indistinguishability using an α- BBO crystal to overlap both the beams. We can use a wavelength division multiplexer to separate signal and idler beams.

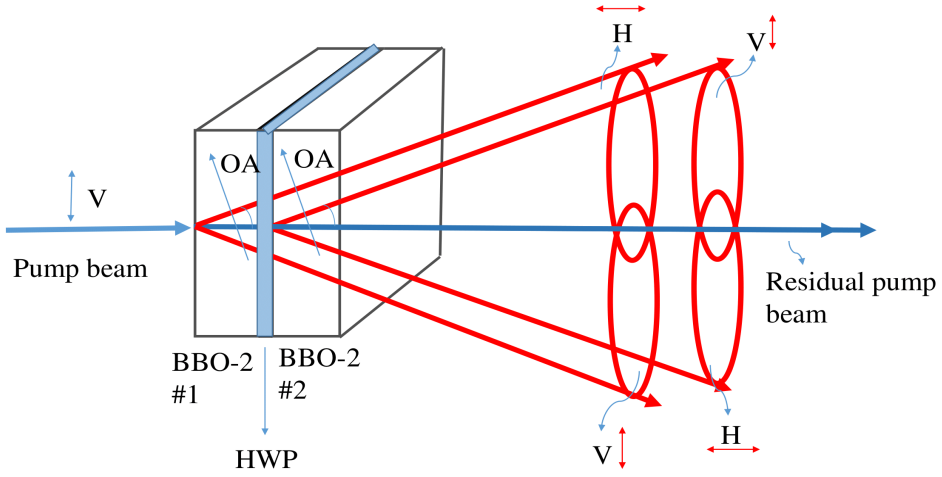

Figure 14: Schematic representation of sandwiched source.

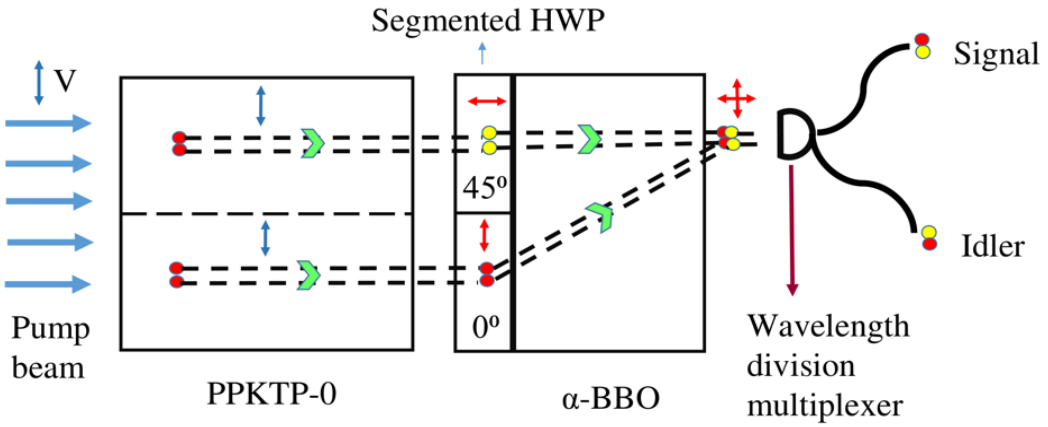

Figure 15: Schematic representation for conversion of position correlated photons to polarization entanglement.

5.3 Single crystal - double pass

Non-collinear schemes

Using two routes for the pump beam within the same crystal is another way to create entanglement.

5.3.1 Rail-cross scheme

In this scheme, the pump photon falls on the crystal and is reflected by using a mirror [33, 34, 37]. The down converted photons are also reflected making sure that they overlap with the second-pass converted photons [Fig :16]. The entangled state is

$$| HH\rangle_1 \pm e^{i\Delta\varphi} | VV\rangle_2$$

where $\Delta\varphi$ is the phase difference due to the optical path length difference.

Variations in this phase shift will also be influenced by changes in the optical path length of the pump and the SPDC photons, and we need to provide interferometric stability to this system.

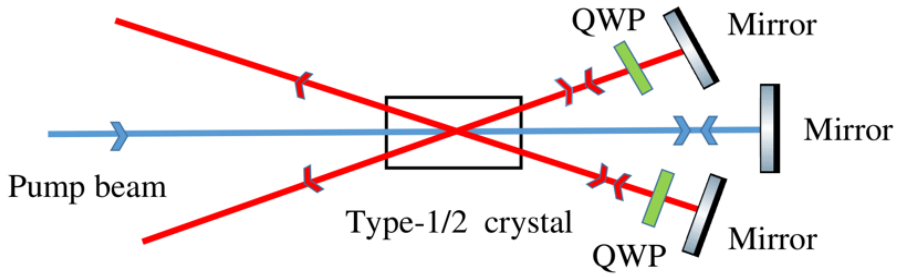

Figure 16: Schematic representation of rail-cross scheme.

5.3.2 Sagnac interferometer

In this scheme, the pump photon is made to fall on the crystal on it's both sides [Fig :17]. The pump beam through one arm produces a signal and an idler beam which are horizontally polarized. From another arm of the loop, the pump beam down converts into signal and idler beam with horizontal polarization which are then converted to two vertically polarized light using an achromatic half waveplate [35, 36]. The down converted photons from both arms interfere with the polarizing beam splitter. This scheme ensures phase stability. In order to remove any kind of walk-off, we need to make sure the crystal is placed symmetrically in the loop.

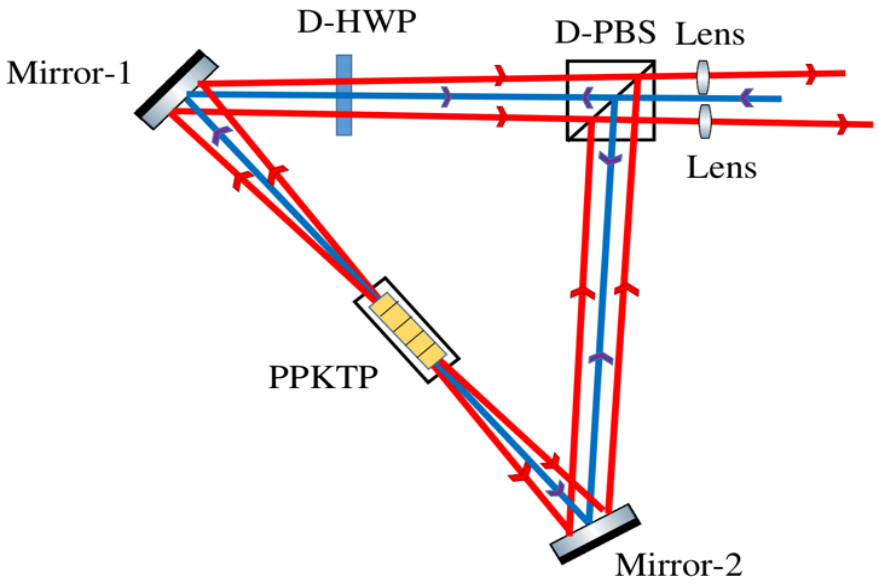

Figure 17: Schematic representation of Sagnac interferometer.

Collinear schemes

5.3.3 Folded Mach-Zehnder

This scheme uses two loops where one loop sends a bidirectional pump beam onto the type-2 crystal and another loop collects down converted photons [Fig :18]. In the latter, one arm has $|HV\rangle$ states whereas in another arm, by using a half wave plate, $|HV\rangle$ is converted to $|VH\rangle$ state. Photons from both arms are made to interfere with a polarising beam splitter. Hence entangled photons are generated. The disadvantage of this scheme is that it has 2 loops [38, 39]. Here, all the emitted photon pairs are polarization entangled irrespective of their wavelengths and directions of emission.

5.3.4 Sagnac configuration

In this scheme, both pump and down converted photons travel the same path and we can use type-0, 1 or 2 phase matching [Fig :20]. Let's take an example of a type-2 phase match condition. A diagonally polarised pump beam is incident on PBS. PBS transmits vertically polarized light and reflects horizontally polarised light. One arm converts $|H\rangle \rightarrow |HV\rangle$ which is passed through HWP to get $|VH\rangle$. In another arm, $|V\rangle \rightarrow |HV\rangle$. Photons from both arms interfere with PBS. This scheme is one of the most widely used schemes and offers great interferometric stability. [40, 41].

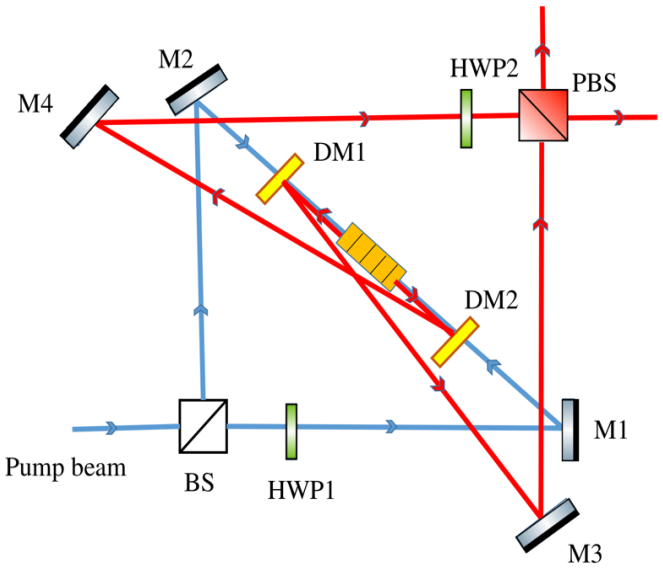

Figure 18: Schematic representation of folded Mach-Zehnder setup.

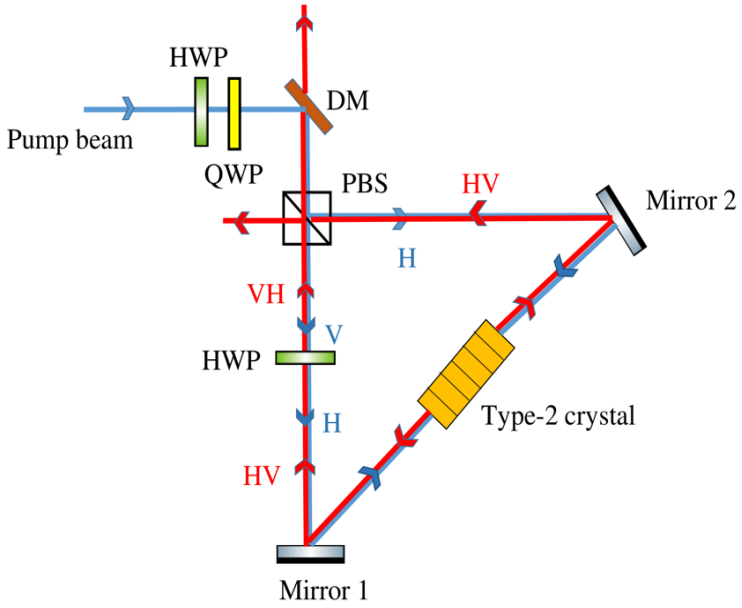

Figure 19: Schematic representation of Sagnac configuration.

5.3.5 Folded sandwich configuration

This configuration has been noted for its brightest source in literature. This scheme has lesser physical footprints than the Sagnac interferometer and also completely utilizes the pump beam. Here [Fig :21], in the first trip, $|V\rangle$ pump beam is down converted to $|VV\rangle$ which is then converted (by QWP) and reflected as $|HH\rangle$. In the second trip, the reflected $|V\rangle$ pump beam is converted to

$|VV\rangle$. Both the converted photons are impinged on YVO_4 crystal which removes spatial walk-offs [42].

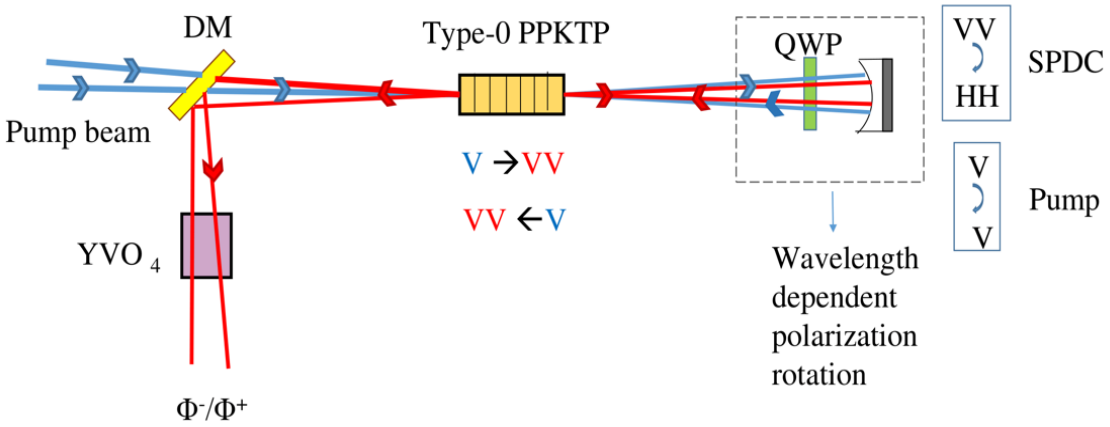

Figure 20: Schematic representation of the folded sandwich configuration.

5.3.6 Linear displacement interferometer

Even in this scheme [Fig :19], pump photons travel through different regions in the crystal. Here the photons are pre-compensated and also post-compensated. We first incident a pre-compensated pump photon onto BBO crystal. Its birefringence property will separate the pump photon into two beams. We are manipulating the polarization of the photons using HWP. Again by using the birefringence property, we are interfering both beams in the BBO cystal. The phase difference is post-compensated using YVO_4 crystal [43].

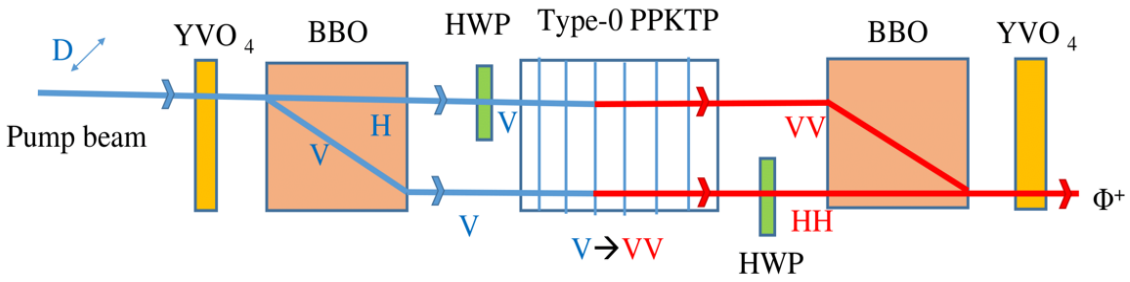

Figure 21: Schematic representation of linear displacement interferometer.

Part III

Methods to characterise entangled photons source

The characterization involves measuring the quantum correlations between the two photons, including their polarization, phase, and spatial modes. Precise control and manipulation of these properties are critical for many quantum information applications, such as quantum key distribution and quantum teleportation.

In this section, we focus on the experimental characterization of entangled photons. Specifically, we investigate the brightness of the entangled photon source, the heralding efficiency, the Hanbury Brown and Twiss (HBT) experiment, the violation of the Clauser-Horne-Shimony-Holt (CHSH) inequality, the visibility of the interference fringes, the polarization correlation measurements, and the reconstruction of the quantum state using quantum state tomography.

6 Methods:

6.1 Brightness

It is defined as the number of photon pairs emitted per unit time, per unit wavelength, per unit solid angle, and per unit area of the crystal. The brightness of the photon pairs directly affects the quality and fidelity of quantum entanglement, making it a crucial metric for many quantum information processing applications [21].

The brightness of entangled photon pairs can be increased by using a variety of techniques. For instance, the use of highly efficient detectors and optimized optical components can reduce the loss of photons and enhance the collection efficiency, leading to higher brightness. Additionally, the use of non-linear crystals with high nonlinearities and small cross-sectional areas can increase the probability of photon pair generation and improve the brightness.

The characterization of entangled photons' brightness requires precise measurement techniques, such as coincidence counting, which involves detecting the coincident arrival of the two entangled photons. The coincidence rate, defined as the number of coincident events per unit time, can be used to determine the brightness of the photon pairs.

The measurement of the brightness can provide important information about the quality of entanglement. For example, a high coincidence rate indicates a high degree of correlation between the

entangled photons, while a low coincidence rate may indicate a poor quality of entanglement due to photon loss or decoherence. Moreover, the brightness can also affect the fidelity of quantum teleportation and quantum cryptography protocols, making it a critical parameter to optimize in these applications.

6.2 Heralding efficiency

It refers to the probability of detecting one of the entangled photons, called the herald photon, and thereby heralding the presence of the other entangled photon [23].

In reality, various factors can cause losses, including the absorption of the crystal, the reflection and scattering of photons, and the inefficiency of detectors. These losses can reduce the heralding efficiency of the process, leading to a lower probability of detecting the entangled photon pair.

6.3 Hanbury Brown -Twiss experiment (HBT)

The source of SPDC must produce single photons that are quantum in nature, and not classical. To verify this, we can employ the second-order correlation function which also ensures that the generated photons exhibit the property of antibunching, meaning they are equally spaced from each other and hence considered single photons [18].

After the down conversion, idler photons are directly sent to a single photon detector which are used as a trigger. Signal photons are sent to fiber based beam splitter whose 2 outputs are connected to single photon detectors. If the electromagnetic fields are classical in nature, then they passes through both the paths in the beam splitter. If they are particles (quantum), then there is 50% probability to pass in either of the two outputs. We record the coincidence counts in all three detectors and calculate the second order correlation function.

Second order correlation function is given by,

$$g^2(\tau) = \frac{\langle I(t)I(t+\tau)\rangle}{\langle I(t)\rangle\langle I(t+\tau)\rangle}$$

where I(t) is the intensity of the light beam and τ is the time delay in the intensity correlation .

Non classical light show sub Poissonian photon statistics and they have,

$$g^2(\tau = 0) < 1$$

6.4 Visibility

The visibility of an interference pattern provides a quantitative measurement of the contrast between the bright and dark fringes produced by the interference of waves [21]. This measure is related to the coherence properties of the light source, and it is particularly useful for investigating the coherence of photons in an interferometer. When multiple waves interfere, they create constructive or destructive interference, depending on their relative phase. The degree of coherence between the waves is a significant factor in determining the visibility of the interference pattern because it affects the probability of constructive interference. In the case of photons, perfect coherence means that they have the same polarization, frequency, and phase. When photons are perfectly coherent, the interference pattern will have high visibility, indicating a high degree of constructive interference. However, if the photons are not perfectly coherent, the interference pattern's visibility will decrease, resulting in a lower degree of constructive interference. Additionally, the visibility of the interference pattern can be used to distinguish between entangled and independent photons. Entangled photons exhibit a higher degree of coherence and visibility, leading to a more pronounced interference pattern compared to independent photons.

The visibility is calculated as :

$$\upsilon = \frac{C_{max} - C_{min}}{C_{max} + C_{min}}$$

Which can be written as ,

$$\upsilon = \frac{P_{HH} + P_{VV} - P_{HV} - P_{VH}}{P_{HH} + P_{VV} + P_{HV} + P_{VH}} \tag{29}$$

where C_{max} and C_{min} are maximal and minimal coincidence count rates. $P_{\alpha\beta}$ is the probability of getting coincidence counts in α and β polarization states.

For an ideal entanglement case, $\upsilon = 1(100\%)$.

6.5 CHSH inequality

To prove the photons are entangled, we will have to first prove they are non local. The property of entangled quantum systems is that upon measuring one quantum system we can predict the properties of the other entangled system. This would imply that the information is being passed between the two systems more than the speed of light but this violates causality. So Einstein, Boris Podolsky and Nathan Rosen (in 1935) [19] argued that the quantum theory is incomplete and there are certain local variables that are hidden in these quantum systems and they are responsible for the property of entanglement. This is the famous EPR paradox and it showed that quantum mechanics

is nonlocal (Locality means that the information between two particles cannot be communicated faster than the speed of light).

John Stewart Bell demonstrated that the local hidden variable theory is inconsistent with the statistical predictions of quantum mechanics by investigating the EPR paradox. To prove Bell's theorem, various tests, known as Bell's inequality tests, have been conducted. The CHSH inequality test is one of the most commonly used tests to verify Bell's theorem.

Let's send a correlated pair of particles to A and B. Let the correlation between the two particles be λ which is locally present but is hidden away from us. Let the value of λ be present in each pair and vary as per the probability distribution $\rho(\lambda)$. A and B's outcomes are a , b ϵ {-1 , 1 } and they follow a probability distribution of A(a, λ) & B(b, λ), where a & b represent the experimental settings of their measuring instruments, which we are free to modify. The expectation value of their outcome is given by:

$$E(a,b) = \int_{\lambda} A(a,\lambda)B(b,\lambda)\rho(\lambda)d\lambda$$

$$E(a_1,b_1) - E(a_1,b_2) = \int_{\lambda} A(a_1,\lambda)B(b_1,\lambda)\rho(\lambda)d\lambda - \int_{\lambda} A(a_1,\lambda)B(b_2,\lambda)\rho(\lambda)d\lambda$$

$$E(a_1,b_1) - E(a_1,b_2) = \int_{\lambda} [A(a_1,\lambda)B(b_1,\lambda) - A(a_1,\lambda)B(b_2,\lambda) \pm A(a_1,\lambda)B(b_1,\lambda)A(a_2,\lambda)B(b_2,\lambda)$$

$$\mp A(a_1,\lambda)B(b_1,\lambda)A(a_2,\lambda)B(b_2,\lambda)]\rho(\lambda)d\lambda$$

$$= \int_{\lambda} [A(a_1,\lambda)B(b_1,\lambda)(1 \pm A(a_2,\lambda)B(b_2,\lambda)) - A(a_1,\lambda)B(b_2,\lambda)(1 \pm A(a_2,\lambda)B(b_1,\lambda))]\,\rho(\lambda)d\lambda$$

Take the absolute values on both sides:

$$|E(a_1,b_1) - E(a_1,b_2)| = \int |A(a_1,\lambda)B(b_1,\lambda)(1 \pm A(a_2,\lambda)B(b_2,\lambda))$$

$$-A(a_1,\lambda)B(b_2,\lambda)(1 \pm A(a_2,\lambda)B(b_1,\lambda))|\rho(\lambda)d\lambda$$

On using the triangle inequality : $|a-b| \leq |a| + |b|$

$$|E(a_1,b_1) - E(a_1,b_2)| \leq \int |A(a_1,\lambda)B(b_1,\lambda)(1 \pm A(a_2,\lambda)B(b_2,\lambda))|$$

$$-|A(a_1,\lambda)B(b_2,\lambda)(1 \pm A(a_2,\lambda)B(b_1,\lambda))|\rho(\lambda)d\lambda$$

As $|A(a,\lambda)B(b,\lambda)| \leq 1$(because maximum value of probability distributions can be 1)

$$|E(a_1,b_1) - E(a_1,b_2)| \leq \int [(1 \pm A(a_2,\lambda)B(b_2,\lambda)) - (1 \pm A(a_2,\lambda)B(b_1,\lambda))]\,\rho(\lambda)d\lambda$$

$$|E(a_1,b_1) - E(a_1,b_2)| \leq \left[\int (1 \pm A(a_2,\lambda)B(b_2,\lambda))\rho(\lambda)d\lambda\right] - \left[\int (1 \pm A(a_2,\lambda)B(b_1,\lambda))\rho(\lambda)d\lambda\right]$$

$$|E(a_1,b_1) - E(a_1,b_2)| \leq 2 - |E(a_2,b_2) - E(a_2,b_1)|$$

$$S = |E(a_1,b_1) - E(a_1,b_2)| + |E(a_2,b_2) + E(a_2,b_1)| \tag{30}$$

$$S = |E(a_1,b_1) - E(a_1,b_2) + E(a_2,b_2) + E(a_2,b_1)| \leq 2$$

Now lets consider the particles to be quantum.

Let Φ_a and Φ_b be the orientation of the polarizers in arms A and B and are kept in the x-z plane [32]. The projection operators of both polarizers are given by :

$$\Pi_a = |n_a^+\rangle\langle n_a^+| - |n_a^-\rangle\langle n_a^-|$$

$$\Pi_b = |n_b^+\rangle\langle n_b^+| - |n_b^-\rangle\langle n_b^-|$$

Let α, β be the angle of orientation for both polarizers. On rewriting the projection operators in Pauli matrices,

$$\Pi_a = \overrightarrow{\sigma}.\overrightarrow{a}\,; \Pi_b = \overrightarrow{\sigma}.\overrightarrow{b}$$

and

$$\overrightarrow{a} = \cos(\alpha)\widehat{x} + \sin(\alpha)\widehat{z}$$
$$\overrightarrow{b} = \cos(\beta)\widehat{x} + \sin(\beta)\widehat{z}$$

The source produces the photon pairs in the state,

$$|\psi\rangle = \frac{1}{\sqrt{2}}\left[|\,H\rangle_1\,|\,H\rangle_2 \pm e^{i\varphi}\,|\,V\rangle_1\,|\,V\rangle_2\right]$$

The joint operator acting on the entire state $|\Psi\rangle$ will be given by:

$$\Pi = \Pi_a \otimes \Pi_b$$

Expectation value of both orientations is given by,

$$E(a,b) = \langle\psi|\Pi_a \otimes \Pi_b|\psi\rangle$$
$$= \frac{\langle HH|\Pi_a \otimes \Pi_b|HH\rangle}{2} + \frac{\langle HH|\Pi_a \otimes \Pi_b|VV\rangle}{2} + \frac{\langle VV|\Pi_a \otimes \Pi_b|HH\rangle}{2} + \frac{\langle VV|\Pi_a \otimes \Pi_b|VV\rangle}{2}$$

Sustituting the values of $\overrightarrow{a}$ and $\overrightarrow{b}$:

$$E(a,b) = \frac{1}{2}[\langle HH|(\cos(\alpha)\overrightarrow{\sigma}_x + \sin(\alpha)\overrightarrow{\sigma}_z) \otimes (\cos(\beta)\overrightarrow{\sigma}_x + \sin(\beta)\overrightarrow{\sigma}_z)|HH\rangle$$

$$+\langle HH|(\cos(\alpha)\overrightarrow{\sigma}_x + \sin(\alpha)\overrightarrow{\sigma}_z) \otimes (\cos(\beta)\overrightarrow{\sigma}_x + \sin(\beta)\overrightarrow{\sigma}_z)|VV\rangle$$
$$+\langle VV|(\cos(\alpha)\overrightarrow{\sigma}_x + \sin(\alpha)\overrightarrow{\sigma}_z) \otimes (\cos(\beta)\overrightarrow{\sigma}_x + \sin(\beta)\overrightarrow{\sigma}_z)|HH\rangle$$
$$+\langle VV|(\cos(\alpha)\overrightarrow{\sigma}_x + \sin(\alpha)\overrightarrow{\sigma}_z) \otimes (\cos(\beta)\overrightarrow{\sigma}_x + \sin(\beta)\overrightarrow{\sigma}_z)|VV\rangle]$$

.

This can be simplified to

$$E(a,b) = \cos(\alpha)\cos(\beta) + \sin(\alpha)\sin(\beta) = \cos(\alpha - \beta)$$

The S parameter can be calculated as,

$$S = |E(a_1,b_1) - E(a_1,b_2) + E(a_2,b_2) + E(a_2,b_1)|$$
$$S = \cos(\alpha_1 - \beta_1) - \cos(\alpha_1 - \beta_2) + \cos(\alpha_2 - \beta_2) + \cos(\alpha_2 - \beta_1)$$

Now, for the choices of $\alpha^1 = 0°, \alpha^2 = 90° and \beta^1 = 45°, \beta^2 = 135°$, we get,

$$S = 2\sqrt{2}$$

So quantum mechanism puts a upper bound of $2\sqrt{2}$ to the value of S. So if the photons are nonlocal and correlated, then they must obey the condition $2 < S \leq 2\sqrt{2}$.

6.6 Polarization correlation measurements

At the polarizers, the state of the down converted photons are in a superposition of both horizontal and vertical photons. If we measure horizontal (/vertical) state in one arm, the superposition state in another arm also collapses to horizontal /vertical state depending on which states have been

entangled. Hence we will get high coincidence counts. If we project non - entangled states on the polarisers, then we will obviously get low coincidence counts. We can use this criteria to assess which all polarization degrees of freedom are entangled.

In general, if $|\alpha\rangle$ is the polarization angle of a polarizer at A and $|\beta\rangle$ is the polarization angle of a polarizer at B, the probability of finding the incoming two photon state, ρ, being projected on to polarization state $|\alpha\beta\rangle$ is given by [44] :

$$p_{\alpha\beta} = Tr\{\rho|\alpha\beta\rangle\langle\alpha\beta|\}$$

If the polarization state of the photon pair is in a pure state $|\Psi\rangle$, then

$$p_{\alpha\beta} = |\langle\alpha\beta|\Psi\rangle|^2\}$$

If the source has produced the state:

$$|\Phi^{\pm}\rangle = \frac{1}{\sqrt{2}}\left[|\, H\rangle_1 \,|\, H\rangle_2 \pm |\, V\rangle_1 \,|\, V\rangle_2\right]$$

So the probability of its projection onto polarization state $|\alpha\beta\rangle$ is given by,

$$p_{\alpha\beta} = |\langle\alpha_1|\langle\beta_2|\Phi^{\pm}\rangle|^2 = \frac{1}{2}|\left[\cos\alpha\cos\beta \pm \sin\alpha\sin\beta\right]|^2$$

$$= \frac{1}{2}\cos^2(\alpha \mp \beta)$$

By looking at the pattern of variations in $p_{\alpha\beta}$, we can find out whether our source has produced the state $|\Phi^+\rangle$ or $|\Phi^-\rangle$.

6.7 Quantum state tomography

Quantum state tomography is a method to characterize the property of an unknown quantum system. We know that measurement destroys the quantum state, hence limiting us from making multiple measurements on the same state to measure all its properties. In this technique, in order to know the complete state of a photon, we perform multiple measurements on an identical ensemble of down converted photons by projecting them onto different bases and hence calculating their probabilities. We use this probabilistic mixture to construct a density matrix which helps in characterizing the entangled photons [22].

Let us look step by step on how to construct a density matrix.

We shall use $|\,00\rangle, |\,11\rangle, |\,01\rangle, 10\rangle$ as the basis states. For a single qubit, we can represent the density matrix as:

$$\hat{\rho} = \frac{1}{2}\sum_{i=0}^{3} S_i \hat{\sigma_i}$$

using the Stokes parameter S and Pauli matrices $\hat{\sigma}$. Stokes parameter can be represented as (where $|\,0\rangle, |\,1\rangle$are basis states):

$$S_0 = P_{|0\rangle} + P_{|1\rangle}$$

$$S_1 = P_{\frac{1}{\sqrt{2}}(|0\rangle+|1\rangle)} - P_{\frac{1}{\sqrt{2}}(|0\rangle-|1\rangle)}$$

$$S_2 = P_{\frac{1}{\sqrt{2}}(|0\rangle+i|1\rangle)} - P_{\frac{1}{\sqrt{2}}(|0\rangle-i|1\rangle)}$$

$$S_3 = P_{|0\rangle} - P_{|1\rangle}$$

where $P_{|\Psi\rangle}$ denotes the probability of measuring the state $|\Psi\rangle$. We can see that S_0 is always 1.

But S parameters are used for orthogonal bases and T parameters which are S-like parameters are used for representing nonorthogonal bases on the Poincare sphere. But the problem is,

$$\hat{\rho} \neq \frac{1}{2}\sum_{i=0}^{3} T_i \hat{\tau_i}$$

W.K.T $S_i \equiv Tr\{\hat{\sigma_i}\hat{\rho}\}$ and similarly $T_i \equiv Tr\{\hat{\tau_i}\hat{\rho}\}$ where $\hat{\tau_i} \equiv |\,\Psi_i\rangle\langle\Psi_i| - |\,\Psi_i^{\perp}\rangle\langle\Psi_i^{\perp}|$

Hence we will have to convert T parameters into the S parameters to construct the density matrix and can use the relation,

$$\begin{pmatrix} T_0 \\ T_1 \\ T_2 \\ T_3 \end{pmatrix} = \frac{1}{2}\begin{pmatrix} Tr\{\hat{\tau_0}\hat{\sigma_0}\} & Tr\{\hat{\tau_0}\hat{\sigma_1}\} & Tr\{\hat{\tau_0}\hat{\sigma_2}\} & Tr\{\hat{\tau_0}\hat{\sigma_3}\} \\ Tr\{\hat{\tau_1}\hat{\sigma_0}\} & Tr\{\hat{\tau_1}\hat{\sigma_1}\} & Tr\{\hat{\tau_1}\hat{\sigma_2}\} & Tr\{\hat{\tau_1}\hat{\sigma_3}\} \\ Tr\{\hat{\tau_2}\hat{\sigma_0}\} & Tr\{\hat{\tau_2}\hat{\sigma_1}\} & Tr\{\hat{\tau_2}\hat{\sigma_2}\} & Tr\{\hat{\tau_2}\hat{\sigma_3}\} \\ Tr\{\hat{\tau_3}\hat{\sigma_0}\} & Tr\{\hat{\tau_3}\hat{\sigma_1}\} & Tr\{\hat{\tau_3}\hat{\sigma_2}\} & Tr\{\hat{\tau_3}\hat{\sigma_3}\} \end{pmatrix}\begin{pmatrix} S_0 \\ S_1 \\ S_2 \\ S_3 \end{pmatrix}$$

Now we shall use the three Strokes parameters as co-ordinate axes in 3D space of the Poincare sphere. It is necessary for all physical states to be contained within a sphere. Pure states are located on the surface, with linearly polarized states positioned on the equator and circular states situated at the poles. Inside the sphere, mixed states can be found, with the center representing a completely unpolarized state or totally mixed state. This arrangement characterizes the location of different types of states within the sphere.

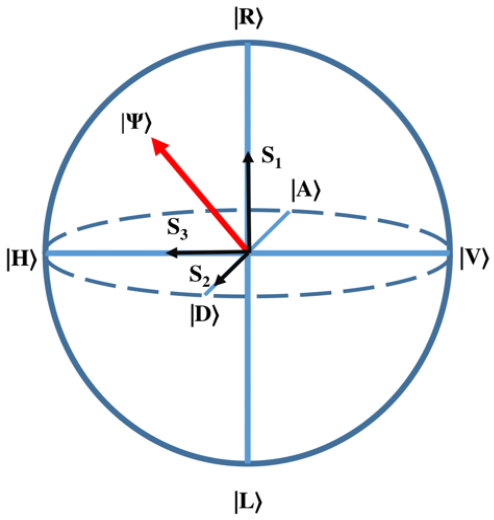

Figure 22: The Bloch Poincare sphere. S_1, S_2, S_3 represent the three orthogonal bases. Different values of S / T refers to different points on the three axes, finally identifying the unknown state.

For a n-qubit state tomography,

$$S_{i_1,i_2,\ldots i_n} = \left(P_{\psi_1} - P_{\psi_1^\perp}\right) \otimes \left(P_{\psi_2} - P_{\psi_2^\perp}\right) \otimes \ldots \otimes \left(P_{\psi_n} - P_{\psi_n^\perp}\right)$$

$$\hat{\rho} = \frac{1}{2^n} \sum_{i_1,\ldots i_n=0}^{3} S_{i_1,\ldots i_n} \hat{\sigma_{i_1}} \otimes \sigma_{i_2} \otimes \hat{\ldots} \otimes \hat{\sigma_{i_n}}$$

We can also represent a given density matrix in the form of a Werner state :

$$\hat{\rho}_W = P|\gamma\rangle\langle\gamma| + (1-P)\frac{1}{4}I$$

where $\langle\gamma|$ is the maximally entangled state; $\frac{1}{4}I$ is the totally mixed state.

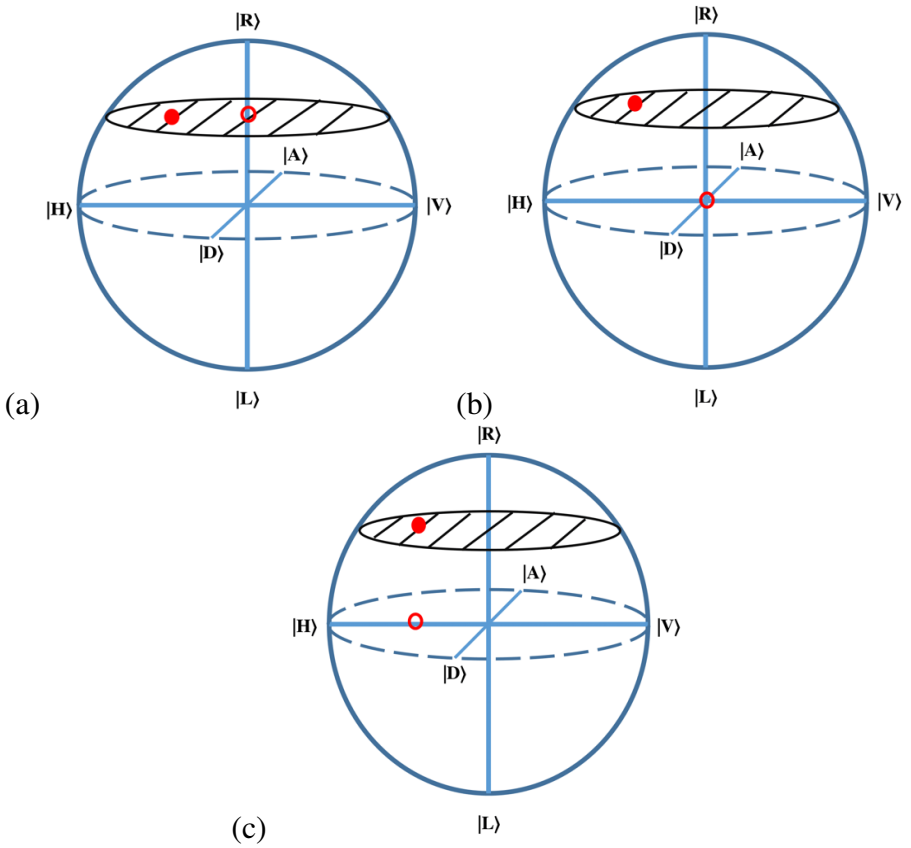

Figure 23: A series of projective measurements on the (a) right-circular (b) diagonal and (c) horizontal axes to identify the unknown state in the Poincare sphere.Red circles are the projective measurements of the unknown state (Darkened red circle).

Errors: real tomography

Tomography of a single-qubit suffers from various sources of errors, such as statistical errors, imperfections in optical components, detection inefficiencies, and drifts in the produced states. These errors affect the estimation of an unknown state by producing a Gaussian error ball instead of a point on the Poincare sphere.

Measurement errors in the basis result in two cones on the Poincare sphere, which meet at the sphere's center. This produces a disc with a certain width on the surface and tapers to a point at the center, converting a plane to a disc with uniform thickness. Statistical errors further affect the knowledge of the unknown state by producing a Gaussian error ball. All the errors that contribute are Gaussian as the photons generation and detection statistics are Gaussian.

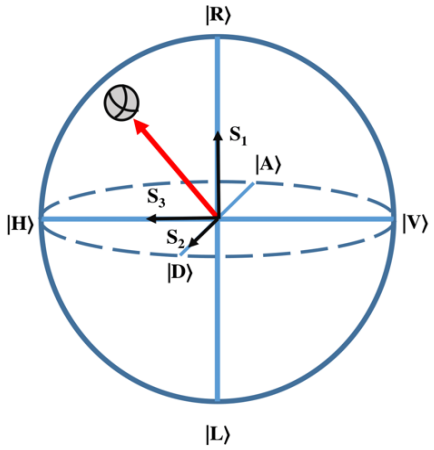

Figure 24: Representation of unphysical state (error ball) on Poincare sphere.

The use of orthogonal bases in tomography is preferred over non-orthogonal bases, as non-orthogonal bases give rise to non-symmetric error balls. Moreover, there is a possibility that the error ball lies outside the sphere, implying the presence of unphysical states. To avoid this, an upper bound is set for the global maximum using the maximum likelihood technique to ensure physical states. In order to obtain physical states through tomography, it is necessary to ensure that the estimated density matrix only contains legally allowed states. To achieve this, it is important to set a maximum value for the likelihood function.

The likelihood function provides information about the unknown state, by assigning probabilities to certain regions of the Poincare sphere. This means that some states are more likely to occur than others, and the likelihood of certain states is more favored than others. This approach allows for the selection of states that are most consistent with the data while excluding unphysical states lying outside the sphere. Therefore, setting a maximum value for the likelihood function is essential to ensure the accuracy and validity of the tomography results.

Firstly, in order for our density matrix to be legal / physical, our matrix must be non-negative - definite - Hermitian density matrix of trace one. So, if any matrix $\hat{A}$ has to be non-negative, then [45],

$$\langle \Psi | \hat{A} \mid \Psi \rangle \geq 0; \forall \mid \Psi \rangle$$

But any matrix which is non-negative definite can be written as :

$$\hat{A} = \hat{B}^{\dagger} \hat{B}$$

On substituting,

$$\langle\Psi|\hat{B}^{\dagger}\hat{B} \mid \Psi\rangle \geq \langle\Psi^{'} \mid \Psi^{'}\rangle \geq 0$$

where $\mid \Psi^{'}\rangle = \hat{B} \mid \Psi\rangle$ and for the matrix to be Hermitian,

$$(\hat{B}^{\dagger}\hat{B})^{\dagger} = \hat{B}^{\dagger}(\hat{B}^{\dagger})^{\dagger} = \hat{B}^{\dagger}\hat{B}$$

To ensure normalization,

$$\hat{g} = \frac{\hat{B}^{\dagger}\hat{B}}{Tr\{\hat{B}^{\dagger}\hat{B}\}}$$

Now, the physical density matrix is given by :

$$\hat{\rho}_p = \frac{\hat{B}^{\dagger}(b)\hat{B}(b)}{Tr\{\hat{B}^{\dagger}(b)\hat{B}(b)\}}$$

b represents $b_i^{'}s$ which are the components of the matrix $\hat{B}$.

Now we need to define a maximum likelihood function.

We will assume that we are using Gaussian counting statistics. If we make a total of Ξ measurements and let m_υ be the number of measurements obtained for υth measurement. The expected values for these measurements on an unknown state $\hat{\rho}_p$ are given by $\bar{m_\upsilon} = \mathcal{N}\langle\Psi_\upsilon \mid \hat{\rho}_p|\Psi_\upsilon\rangle$ where $\mathcal{N}$ is the unknown normalization value. As the number of measurements made is not specific, we define $\mathcal{N}$=$\frac{n_\upsilon}{P_\upsilon}$ .The probability of obtaining m_υ from $\hat{\rho}_p$ is given by :

$$P(m_1, m_2, ..m_\Xi) = \frac{1}{\mathcal{N}}\prod_{\upsilon} exp\left[\frac{-(\bar{m_\upsilon} - m_\upsilon)^2}{2\hat{\sigma}_\upsilon^2}\right]$$

Thus the likelihood that the matrix $\hat{\rho}_p(b_1, b_2, ...b_{m^2})$ could produce the measured data $(b_1, b_2, ..b_\Xi)$ is :

$$P(b_1, b_2, ..b_\Xi) = \frac{1}{Norm}\prod_{\upsilon} exp\left[\frac{-(\mathcal{N}\langle\Psi_\upsilon \mid \hat{\rho}_P(b_1,b_2,...b_{m^2})|\Psi_\upsilon\rangle - m_\upsilon)^2}{2\mathcal{N}\langle\Psi_\upsilon \mid \hat{\rho}_P(b_1,b_2,...b_{m^2})|\Psi_\upsilon\rangle}\right]$$

where Norm is the normalization constant and

$$\bar{m_\upsilon}(b_1, b_2, ...b_{m^2}) = \mathcal{N}\langle\Psi \mid \hat{\rho}_P(b_1, b_2, ...b_{m^2})|\Psi_\upsilon\rangle$$

We can maximise the above probability function or take a minimum of negative of log of the above

equation.As $\mathcal{N}$ is unknown, we define $b'_i = \mathcal{N} b_i$.

$$\mathcal{L}(b'_1, b'_2, ...b'_{m^2}) = \sum_{\upsilon} \left[\frac{(\langle \Psi_\upsilon \mid \hat{\rho}_P(\mathrm{b}'_1,\mathrm{b}'_2,...\mathrm{b}'_{m^2})|\Psi_\upsilon\rangle - m_\upsilon)^2}{2\langle \Psi_\upsilon \mid \hat{\rho}_P(\mathrm{b}'_1,\mathrm{b}'_2,...\mathrm{b}'_{m^2})|\Psi_\upsilon\rangle} + \frac{\log(\langle \Psi_\upsilon \mid \hat{\rho}_P(b'_1, b'_2, ...b'_{m^2})|\Psi_\upsilon\rangle)}{2} \right]$$

We need to numerically minimize this function and find the values for $b'_{i's}$. This is the maximum likelihood function. The density matrix constructed out of these $b'_{i's}$ will give us physical states only.

The next question we need to answer is, how can we characterize the photons using a density matrix?

1] **Fidelity :** It is a measure of how close the experimentally constructed density matrix is to the theoretically derived density matrix. Fidelity is given by :

$$F(\rho_1, \rho_2) = (Tr\{\sqrt{\sqrt{\rho_1}\rho_2\sqrt{\rho_1}}\})^2$$

where ρ_1, ρ_2 are theoretical and experimentally calculated denity matrix.

2] **Concurrence:** It is a measure of the degree of entanglement for two-qubit systems. It is defined as:

$$C = max\{0, \sqrt{a_1} - \sqrt{a_2} - \sqrt{a_3} - \sqrt{a_4}\}$$

where $a'_i s$ are the eigenvalues of the non - Hermitian matrix $\widehat{A}$ which can be arranged in decreasing order as $a_1 \geq a_2 \geq a_3 \geq a_4$.

$\widehat{A}$ is defined as :

$$\hat{A} = \hat{\rho}\hat{\Sigma}\hat{\rho}^T\hat{\Sigma}$$

where $\hat{\Sigma}$ is the spin flip matrix given by :

$$\hat{\Sigma} = \begin{pmatrix} 0 & 0 & 0 & -1 \\ 0 & 0 & 1 & 0 \\ 0 & 1 & 0 & 0 \\ -1 & 0 & 0 & 0 \end{pmatrix}$$

For product states, the concurrence ranges from 0 to a maximum value of 1 for Bell states.

3] **Linear entropy:** The linear entropy quantifies the degree of mixture in a quantum state. The linear entropy for a two-qubit system is defined by:

$$S_L = \frac{1}{4}(1 - Tr(\hat{\rho}^2))$$

S_L ranges from 0 for pure states to 1 for a completely mixed state.

4] **Purity:** Purity is a crucial measure of entangled photons that characterizes the degree of correlation between the entangled state and the mixed state. It provides valuable information about the degree of entanglement and the amount of noise and decoherence present in the system. The purity of the entangled photon state can be quantified using the density matrix formalism

$$P = Tr(\rho^2)$$

The purity ranges between 0 and 1, where a value of 1 corresponds to a pure state, while a value of 0 corresponds to a maximally mixed state.

Measuring both purity and linear entropy can offer a comprehensive understanding of the behavior of the entangled photons. In particular, when observing a high level of entanglement between the photons alongside a low level of purity, this implies that the photons are combined with other states, thereby degrading their quantum coherence. Conversely, if a low level of entanglement is observed between the photons, but a high level of purity is detected, this suggests that the photons are not entangled, but their quantum coherence remains intact.

Part IV

Experimental generation and characterisation of entangled photons source

7 Experimental setup on the generation of entangled photons

Figure 25 depicts a schematic diagram of the experimental setup used to generate polarization-entangled photons. The apparatus consists of a pump laser with 15mW power and 405nm wavelength that incidents a vertical beam of photons onto a crossed type-1 BBO crystal after passing through a half waveplate and a precompensation crystal [YVO_4]. The down converted photons of degenerate wavelengths of 810nm are emitted at a half opening angle of 3° which are passed into a post compensation crystal [YVO_4]. Later a long pass filter is used to block pump photons and pass only the signal and idler beam into polarisers which are then collected by the fiber collimators to pass through the polarization maintaning fibers to direct them on the avalanche photodiodes (APD) in the coincidence logic counter. We have used quED - Entanglement Demonstrator from qutools to perform the experiment [Fig :26].

If we look at the down conversion process closely, we are using a type-1 crossed BBO crystal. So the incident photon must be diagonally polarised. Detailed mechanism of down conversion in crossed type-1 crystal is explained in chapter 2. Hence we are placing a HWP oriented at 22.5° to the vertical polarization of the laser source. To differentiate between horizontal and vertical photons, a pre-compensation crystal [YVO_4] was employed, which introduced a slight delay between them so that both photons incident simultaneously on both the BBO crystals. First crystal down converts vertically polarised pump beam to horizontally polarised signal and idler beam; second crystal down converts horizontally polarised pump beam to vertically polarised signal and idler beam. The two down converted cones are made to overlap with each other using a post compensation crystal [YVO_4] which removes spatial and temporal walk - offs. We can choose any two diametrically opposite points to obtain the polarization entangled state :

$$| H\rangle_1 \, | H\rangle_2 \pm e^{i\varphi} \, | V\rangle_1 \, | V\rangle_2.$$

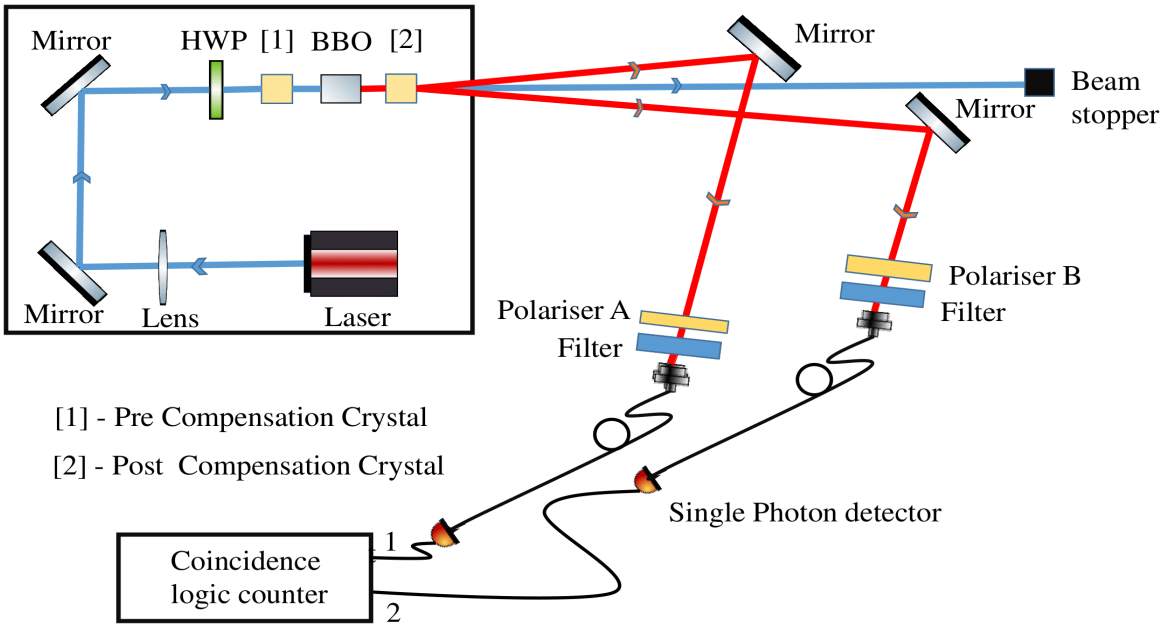

Figure 25: Schematic representation of entangled photons source.

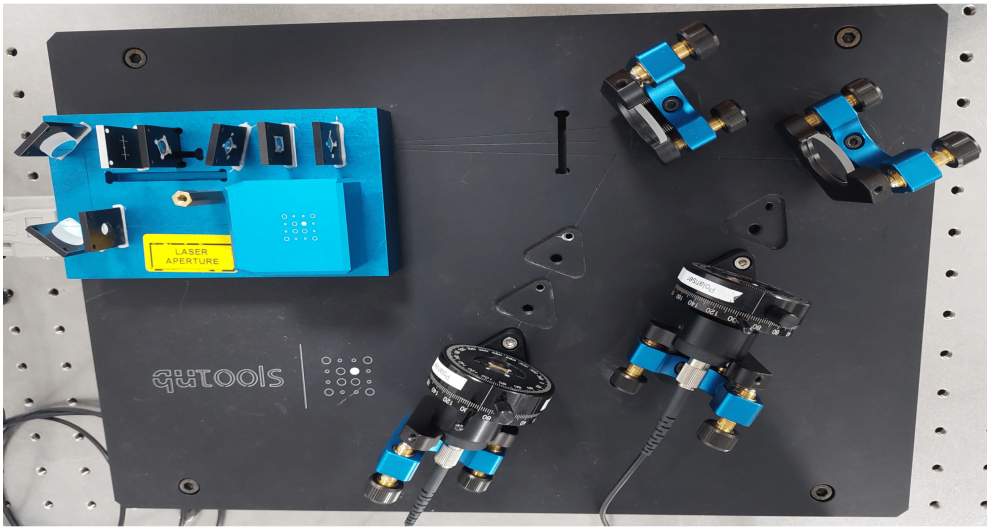

Figure 26: Experimental setup on generation of entangled photons.

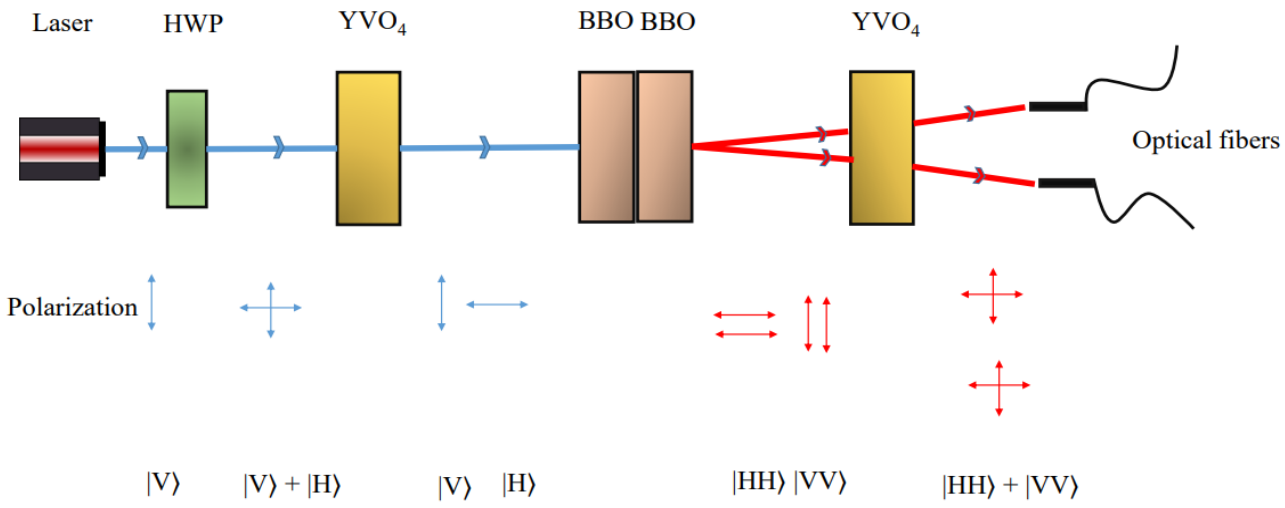

Figure 27: Schematic representation of generation of entangled photons in our setup.

8 Experimental results on the characterization of entangled photons source

1.Brightness :

Brightness = Number of coincidence counts/s/mW

Experimental result:

Brightness = 114.92 cps/mW

2.Heralding efficiency:

Heralding efficiency is the ratio of observed coincidence counts to the single counts of signal/idler counts.

Experimental result:

Heralding efficiency = 0.0756

We have obtained 7.5% heralding efficiency.

3.HBT experiment:

Experimental procedure :

The down converted photons are directly passed into the long pass filters to incident them on the single photon detectors. As the detectors measure coincidence counts, we can write the second order correlation in terms of probabilities as (for $\tau = 0$ case) :

$$g^2(0) = \frac{P_{t12}}{P_{t1}P_{t2}}$$

where P_{t12} is the probability of measuring coincidence counts in all three detectors simultaneously. $P_{t1/2}$ is probability of finding coincidence counts in trigger and 1^{st} or 2^{nd} detector. Probabilities can be expressed in terms of triple coincidences as $P_{t12} = \frac{N_{t12}}{N_t}$ and double coincidences N_{t1}, N_{t2} . So,

$$g^2(0) = \frac{N_{t12}N_t}{N_{t1}N_{t2}}$$

N_t is the single count of the trigger (idler) detector.

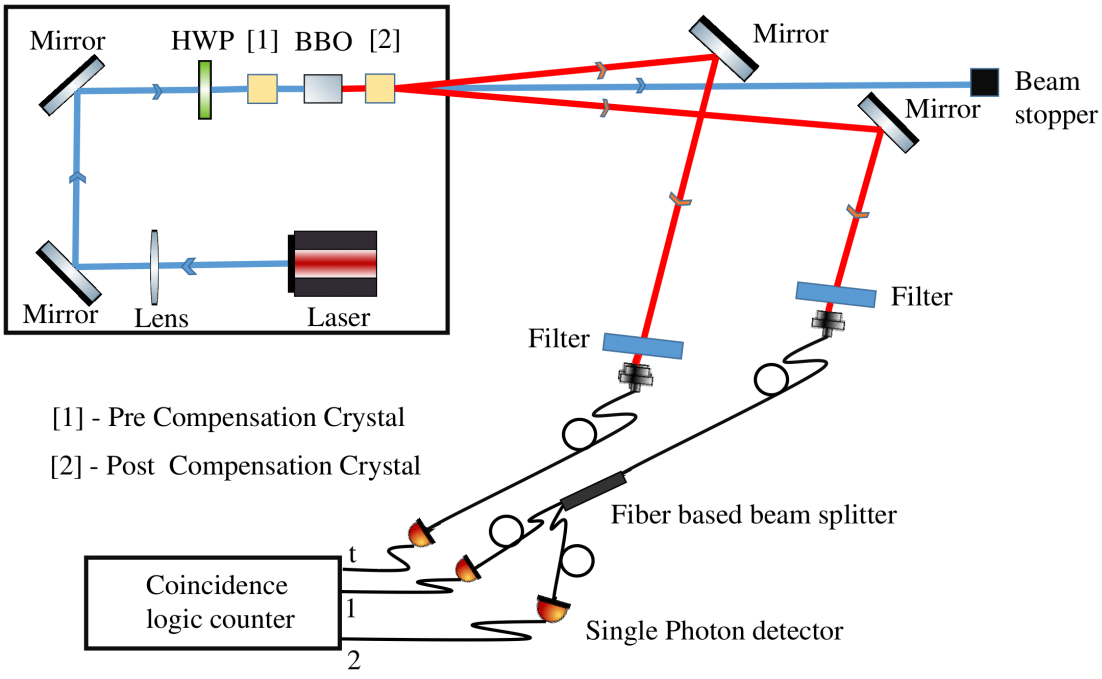

Figure 28: Schematic of HBT experiment

Experimental result:

In our experiment, the obtained value of $g^2(0) = 0.003919 \pm 0.003$, which is less than 1, supports the fact that the photons are quantum in nature and have spatial coherence. Hence the source produces single photons.

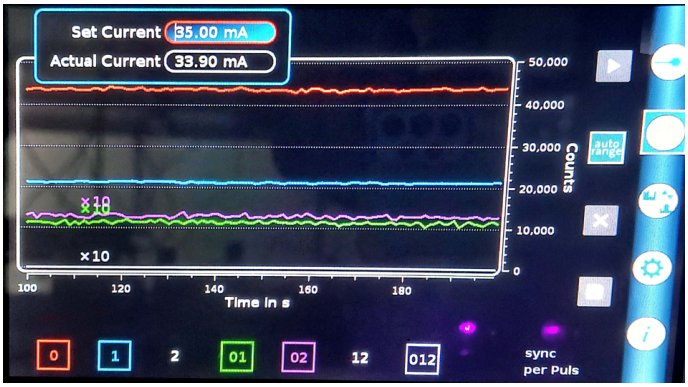

Figure 29: Experimental data of HBT experiment.

The three detectors are connected to the control unit of Qutools. This image is displayed on Qutools control unit screen showing the triple coincidence counts (white line) ; single counts of trigger channel (orange line) and first detector (blue line); double coincidence counts of trigger and first detector (green line) , trigger and second detector (pink line).

4.Visibility:

Experimental procedure:

Set the polarizers in both the arms at (H, H), (V, V), (V, H), (H, V) polarization states and note down their coincidence counts. Use the visibility formula given in the equation.29 to estimate the available pairs of entangled photons.

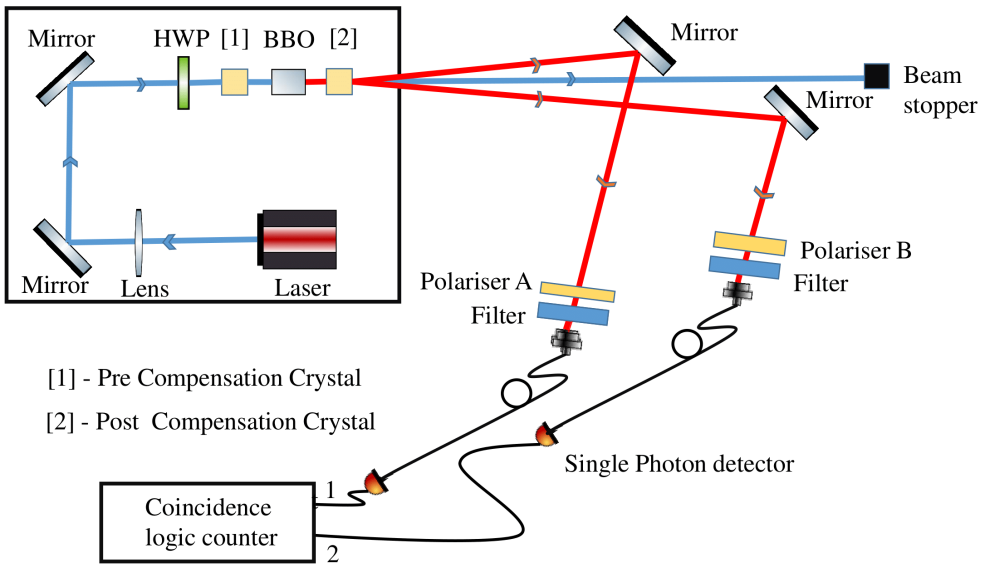

Figure 30: Optical schematic for visibility measurement.

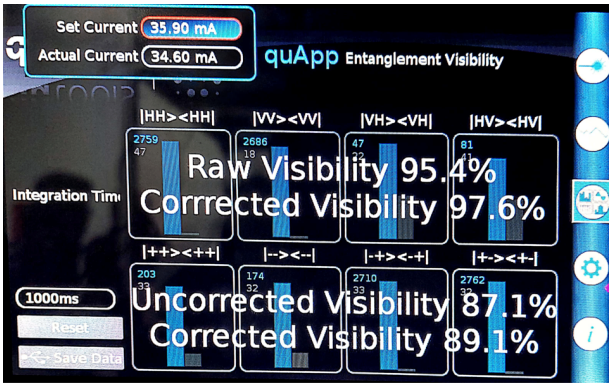

Figure 31: Experimental data of visibility.

Experimental result:

Experimentally, we have obtained visibility of 97.6% in H-V basis and 89.1% in D-A basis.

5.CHSH inequality:

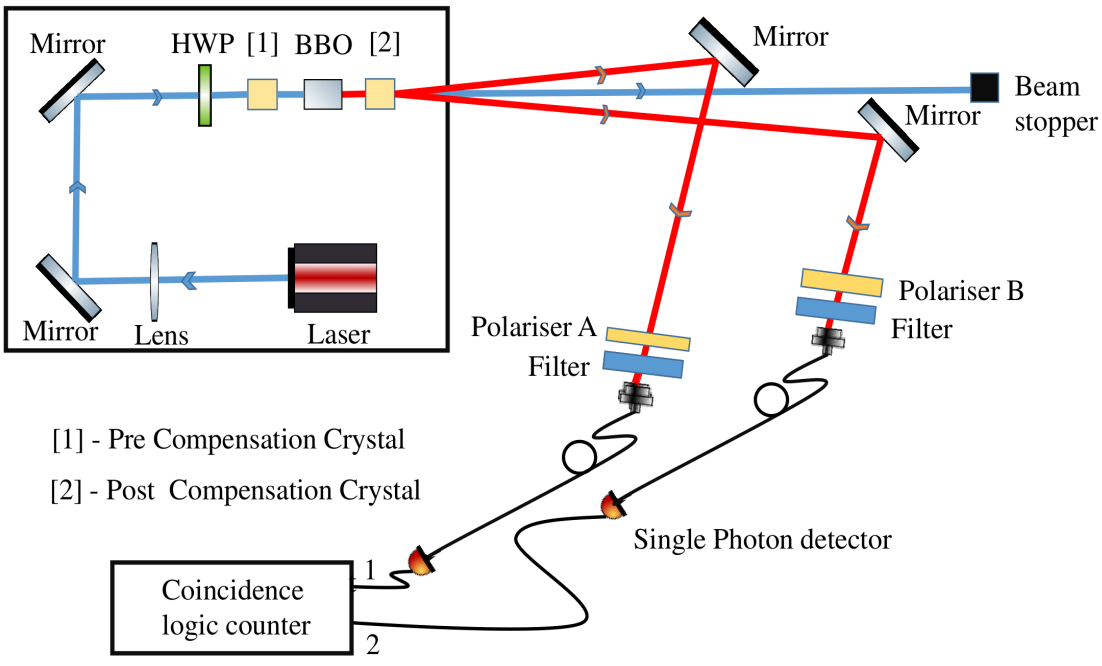

Figure 32: Schematic for CHSH inequality

Experimental procedure:

The polarizer for the signal beam is set at two angles (a, a') and similarly, for the idler beam, we set (b, b') in the polarizer. We can make 4 pairs of combinations of polarizers $[(a,b),(a,b'),(a',b),(a',b')]$ out of these four angles. For each pair of these combinations, the expectation values are calculated as ,

$$E(a_1,b_1) = \frac{C(a_1,b_1) - C(a_1,b_1^{\perp}) - C(a_1^{\perp},b_1) + C(a_1^{\perp},b_1^{\perp})}{C(a_1,b_1) + C(a_1,b_1^{\perp}) + C(a_1^{\perp},b_1) + C(a_1^{\perp},b_1^{\perp})}$$

where $C(a_1,b_1)$ are the coincidence counts. $a_1^{\perp}, b_1^{\perp}$ are the perpendicular directions to a , b. So we require 16 pairs of basis to evaluate the S parameter. We can calculate the S value by,

$$S = |E(a_1,b_1) - E(a_1,b_2) + E(a_2,b_2) + E(a_2,b_1)| \leq 2\sqrt{2}$$

Experimental result:

Experimentally we have obtained S = 2.629±0.021 which is within the range $2 < S \leq 2\sqrt{2}$. Hence the generated photons are non local.

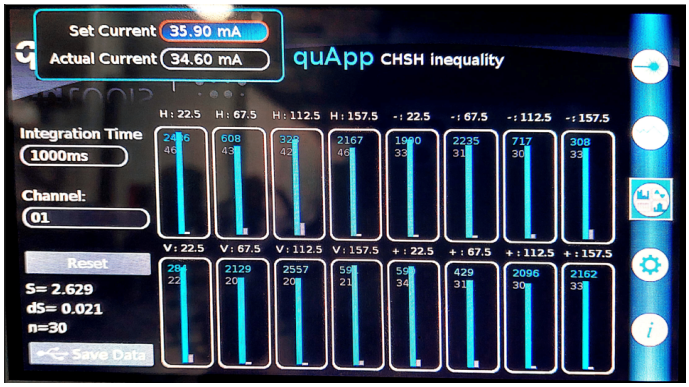

Figure 33: Experimental data for CHSH inequality.
Coincidence counts for all 16 basis choices has been displayed.

6.Polarization correlation measurements :

Experimental procedure:

We consider any four bases of our choice for polariser A and rotate the polariser B in 360° for every basis choice and look at the variations in their coincidence counts by plotting them on a graph. We have chosen horizontal, vertical, diagonal and antidiagonal basis for polariser A and concidence counts for every 10° rotation of polariser B is noted.

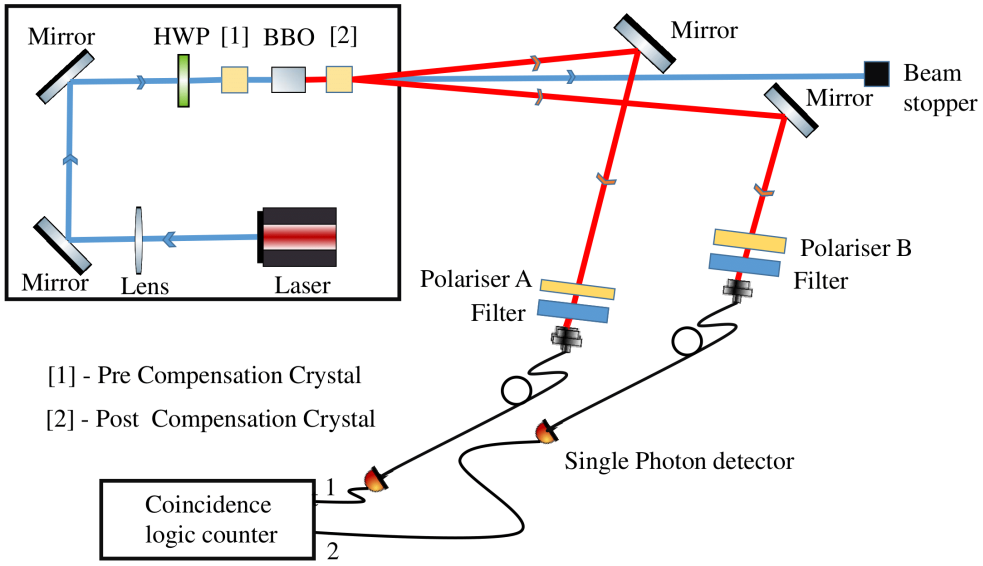

Figure 34: Schematic for polarization correlation measurements.

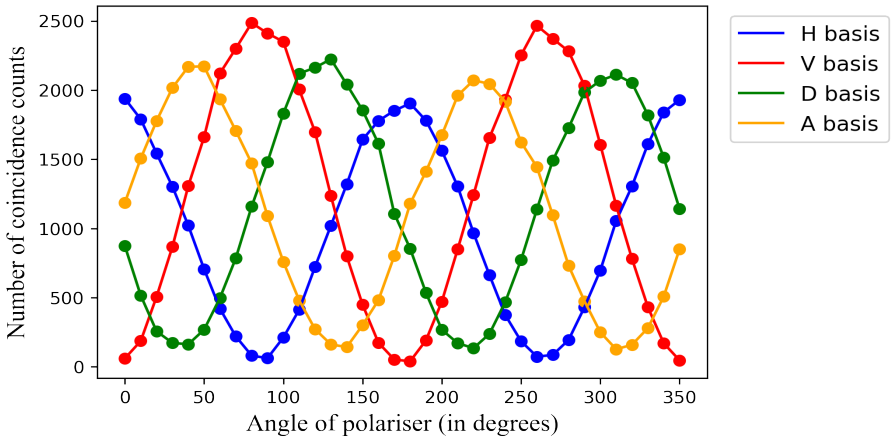

Figure 35: Experimental Data for polarization correlation measurement.
We can assess the level of entanglement in different polarization states.

Experimental result :

We can see from the graph, figure 35 that the curves follow the pattern $\cos^2(\alpha+\beta)$. Hence we can conclude that $|\Phi^-\rangle$ Bell state has been generated where

$$|\Phi^-\rangle = \frac{1}{\sqrt{2}}\left[|\,H\rangle_1\,|\,H\rangle_2 - |\,V\rangle_1\,|\,V\rangle_2\right].$$

7.Quantum state tomography :

Now let's see how to make these measurements experimentally.

We shall use a quarter wave plate, polarizer and single photon detector in both arms to make polarization measurements [Fig:36]. Quarter waveplate is used to project the unknown state on to circular basis states. Based on various configurations given in Table 2 , we shall note down the coincidence counts for various basis states. We can calculate the Stokes parameter and hence density matrix out of it. We shall apply maximum likelihood technique on the desity matrix to make sure we get physical states.

Projection on to the basis	Angle of QWP	Angle of polariser
$\|H\rangle$	0°	0°
$\|V\rangle$	0°	90°
$\|D\rangle$	45°	45°
$\|A\rangle$	45°	−45°
$\|R\rangle$	45°	90°
$\|L\rangle$	45°	0°

Table 2: Polarization analysis setup.

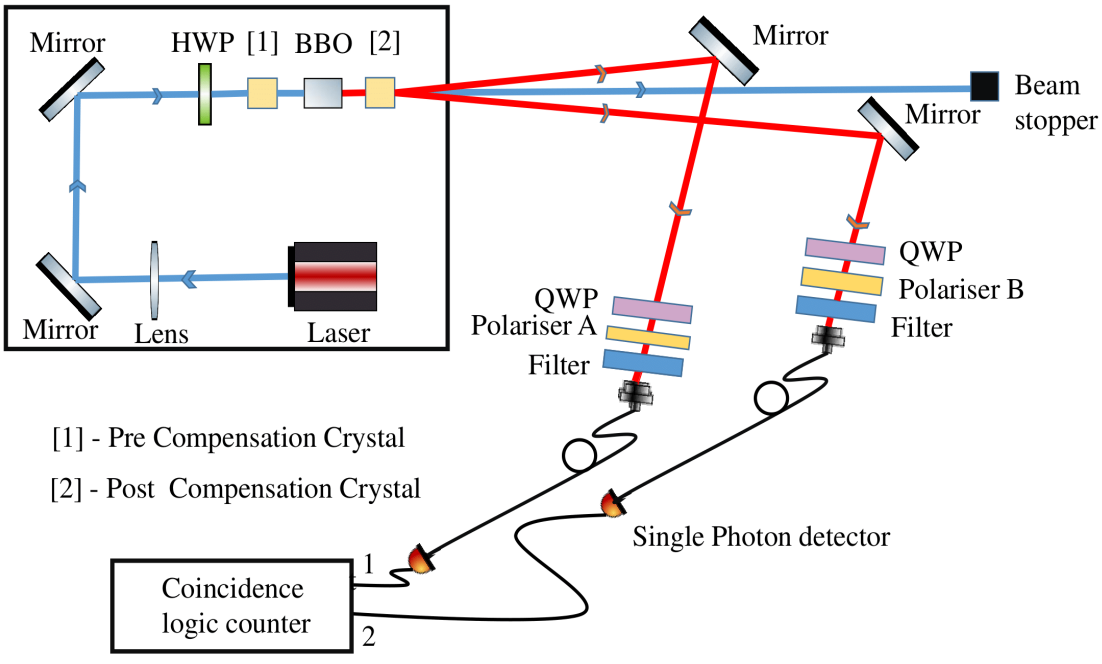

Figure 36: Schematic of Quantum state tomography

	H	V	D	A	R	L
H	1987	83	1540	582	663	1391
V	51	2543	693	1804	1622	924
D	1217	1025	531	1720	395	1834
A	735	1523	1700	509	1811	421
R	672	1605	389	1818	152	574
L	1280	913	1938	374	515	1695

Table 3: Experimental data of quantum state tomography.
Coincidence counts for various basis has been noted.

Experimental results:

We have experimentally obtained the density matrix to be :

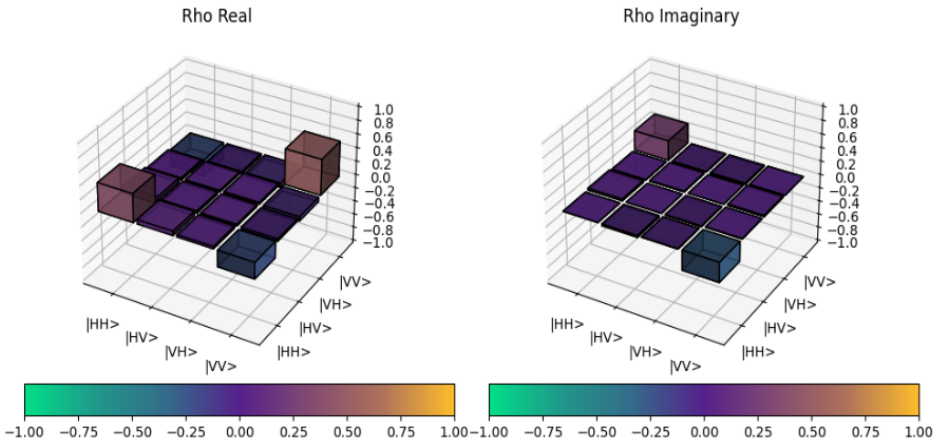

Figure 37: Tomographically obtained density matrix.

$$\rho = \begin{bmatrix} 0.416 & 0.0609 + i0.0263 & 0.0315 + i4.65e-03 & -0.239 + i0.289 \\ 0.0609 - i0.0263 & 0.034 & 0.0239 + i0.0114 & -0.0312 - i6.86e-03 \\ 0.0315 - i4.65e-03 & 0.0239 - i0.0114 & 0.0247 & -0.0617 - i0.0195 \\ -0.239 - i0.289 & -0.0312 + i6.86e-03 & -0.0617 + i0.0195 & 0.524 \end{bmatrix}$$

Eigen Values : 0.85751 , 0.14249 , 0.0 , 0.0

From this density matrix we can estimate the following quanities:

1. Fidelity = 0.71 ± 0.0012
2. Concurrence = 0.708 ± 0.003

3. Linear entropy = 0.244 ± 0.0026

4. Purity = 0.755 ± 0.0015

The fidelty of 0.71 indicates that there is 71% overlap between experimentally constructed density matrix ρ to the theoretically derived density matrix $|\Phi^-\rangle\langle\Phi^-|$. The concurrence of 0.708 indicates that the entangled photons have a significant degree of entanglement, but not perfect entanglement. The linear entropy of 0.244 indicates that the entangled photons are in a relatively pure state and a certain amount of noise is present in the system. The purity of 0.755 suggests that the entangled photons are not maximally mixed, which is consistent with the relatively low value of linear entropy.

Hence we can conclude that the source is generating moderately entangled photons but not maximally entangled Bell states.

Due to the nonlocal correlations, entangled photons are a valuable resource in quantum communication and cryptography which allow for the implementation of protocols that are provably secure against eavesdropping and make possible tasks that are impossible with classical resources.

Quantum key distribution (QKD) [46, 47] is a well-known application of entangled photons, where two parties use quantum states to establish a secret key for encryption. In entanglement-based QKD protocols, Alice and Bob share a pair of entangled photons, using the correlations between their measurements to establish a shared secret key that is secure against eavesdropping. Entangled photons can also be used for quantum teleportation [5, 50], a process that involves transferring the quantum state of a particle from one location to another without physically moving the state itself.

Additionally, entangled photons can be used for quantum random number generation (QRNG) [48, 49], a process for generating truly random numbers using quantum states. The measurement outcomes of entangled photons are truly random and unpredictable, making them ideal for QRNG applications. Lastly, entangled photons can be used for quantum dense coding [51, 52], a process for transmitting two classical bits of information using only one qubit. Alice and Bob share an entangled pair of photons and use measurements to send and receive information efficiently.

Part V

Summary and outlook

In this thesis, we have seen various schemes that can be used to generate entangled photons using nonlinear crystals. We have used crossed type-1 BBO crystal to generate the entangled state

$$|\Phi^-\rangle = \frac{1}{\sqrt{2}} \left[|\, H\rangle_1 \,|\, H\rangle_2 - |\, V\rangle_1 \,|\, V\rangle_2 \right].$$

The entangled photon source exhibits a CHSH parameter of 2.629±0.021, indicating a violation of the Bell inequality. The visibility is higher in the HV basis (94%) than in the AD basis (89%), and the HBT value is 0.003919, indicating low photon bunching. The source has a high brightness (114 cps/mW) but low heralding efficiency (7.5%). The relatively large standard deviation (21) suggests some noise in the system. Overall, the source can produce entangled photons, with desirable properties for quantum information processing, but may have limitations in practical applications due to low heralding efficiency. We conducted polarization correlation measurements to assess the level of entanglement in different polarization states.

The fidelity of 0.71 says that there is only 71% overlap between the theoretically derived density matrix $|\Phi^-\rangle\langle\Phi^-|$ and experimentally constructed density matrix. The concurrence value of 0.708 confirms that the state is entangled. It implies that the two qubits are strongly correlated, and their states are interdependent, even when they are separated by a large distance. This suggests that there may be some noise or errors present in the system, which can affect the degree of entanglement. The purity value of 0.755 indicates that the state is not maximally mixed, meaning that it is not a completely random state. This is consistent with the presence of entanglement in the system, as entangled states are typically not completely random. The linear entropy is a measure of the degree of entanglement in a quantum system. It quantifies the degree of mixedness or impurity in the system, with a value of zero indicating a pure state and a value of one indicating a completely mixed state. The linear entropy value of 0.244 suggests that the state is moderately entangled, as this value is greater than zero but less than the maximum value of 1.

The generation of entangled photon pairs in BBO crystals is limited by non-linear processes, resulting in a low yield of entangled photons. The degree of entanglement in SPDC sources can be degraded by crystal imperfections, pump beam fluctuations, detector inefficiencies, and photon losses. Imperfections in the nonlinear crystal can cause photon pairs to be emitted with different

frequencies, polarizations or spatial modes, reducing correlation between the photons. Fluctuations in the pump beam intensity, duration or spatial profile can lead to variations in the phase-matching conditions and emission cones, affecting entanglement. Detector inefficiencies and photon losses due to absorption, scattering or other environmental interactions can reduce the number of entangled photon pairs and introduce noise, degrading the observed entanglement. Moreover, precise alignment and stabilization of the optical setup is necessary.

In order to increase the efficiency of photon generation, we can use various alternative sources of entangled photons, such as periodically poled crystals (PPKTP , PPLN) which can provide a high degree of tunability in the wavelengths of the entangled photons produced. Another method is using a nonlinear waveguide, where the photons are confined to a small area, leading to a higher photon pair production rate. Photonic crystal fibers, which confine the photons to a hollow core, can also be used to generate entangled photons. In addition, optical fibers doped with rare-earth ions, such as erbium, can also generate entangled photon pairs via SPDC. To increase the detection efficiency of the current setup, superconducting nanowire single photon (SNSP) detectors can be utilized. The anisotropy in correlations between the HV and AD basis may be due to the geometry of the experimental setup, which can be optimized through better optical alignment to improve the overall degree of entanglement.

The future of entangled photons is promising, as they offer a powerful tool for quantum communication and information processing. With the development of advanced techniques for producing and detecting entangled photons, researchers are exploring new applications and potential breakthroughs in areas such as cryptography, sensing, and metrology. The use of entangled photons for secure communication, such as quantum key distribution, is particularly promising, as it allows for the creation of unhackable communication channels. In addition, entangled photons can be used for quantum metrology, enabling high-precision measurements beyond the limits of classical methods. Moreover, the emergence of new materials and technologies for generating and manipulating entangled photons, such as quantum dot arrays and on-chip waveguides, is opening up new avenues for research and development. Overall, the future of entangled photons is bright, with significant potential for revolutionizing the way we communicate and process information.

References

[1] A. Einstein, N. Rosen, and B. Podolsky, "Can quantum-mechanical description of physical reality be considered complete?," Phys. Rev., vol. 47, pp. 777-780, May 1935.

[2] J. S. Bell, "On the Einstein Podolsky Rosen paradox," Physics Physique Fizika, vol. 1, no. 3, pp. 195, 1964.

[3] A. Aspect, J. Dalibard, and G. Roger, "Experimental test of Bell's inequalities using time-varying analyzers," Phys. Rev. Lett., vol. 49, no. 25, pp. 1804-1807, Dec. 1982.

[4] G. Weihs, T. Jennewein, C. Simon, H. Weinfurter, and A. Zeilinger, "Violation of Bell's inequality under strict Einstein locality conditions," Phys. Rev. Lett., vol. 81, no. 23, pp. 5039-5043, Dec. 1998.

[5] C. H. Bennett, G. Brassard, C. Crépeau, R. Jozsa, A. Peres, and W. K. Wootters, "Teleporting an unknown quantum state via dual classical and Einstein-Podolsky-Rosen channels," Phys. Rev. Lett., vol. 70, no. 13, pp. 1895-1899, Apr. 1993.

[6] D. Bouwmeester, J.-W. Pan, K. Mattle, M. Eibl, H. Weinfurter, and A. Zeilinger, "Experimental quantum teleportation," Nature, vol. 390, no. 6660, pp. 575-579, Dec. 1997.

[7] C. H. Bennett and G. Brassard, "Quantum cryptography: Public key distribution and coin tossing," in Proceedings of IEEE International Conference on Computers, Systems and Signal Processing, Bangalore, India, Dec. 1984, pp. 175-179.

[8] N. Gisin, G. Ribordy, W. Tittel, and H. Zbinden, "Quantum cryptography," Rev. Mod. Phys., vol. 74, no. 1, pp. 145-195, Jan. 2002.

[9] J. Abadie et al., "A gravitational wave observatory operating beyond the quantum shot-noise limit," Nature Physics, vol. 7, no. 12, pp. 962-965, Dec. 2010.

[10] LIGO Scientific Collaboration, "A gravitational wave observatory operating beyond the quantum shot-noise limit: Design and quantum noise effects," Classical Quantum Gravity, vol. 28, no. 9, p. 094001, May 2011.

[11] M. A. Nielsen and I. L. Chuang, Quantum Computation and Quantum Information, Cambridge, U.K.: Cambridge Univ. Press, 2000.

[12] J. Preskill, "Quantum computing in the NISQ era and beyond," Quantum, vol. 2, p. 79, Aug. 2018.

[13] Pittman, T. B., Shih, Y. H., Strekalov, D. V., & Sergienko, A. V. (1995). Optical imaging by means of two-photon quantum entanglement. Physical Review A, 52(5), R3429-R3432.

[14] Gatti, A., Brambilla, E., Bache, M., & Lugiato, L. A. (2004). Correlated imaging, quantum and classical. Physical Review A, 70(1), 013802.

[15] Murti, Y. V. G. S., & Vijayan, C. (2014). Essentials of nonlinear optics. John Wiley & Sons.

[16] Kwiat, P. G., Mattle, K., Weinfurter, H., Zeilinger, A., Sergienko, A. V., & Shih, Y. H. (1995). New high-intensity source of polarization-entangled photon pairs. Physical Review Letters, 75(24), 4337-4341.

[17] Loudon, R. (2000). The quantum theory of light (3rd ed.). Oxford University Press.

[18] Hanbury Brown, R. and Twiss, R. Q., "A test of a new type of stellar interferometer on Sirius," Nature, vol. 178, no. 4537, pp. 1046-1048, 1956.

[19] Clauser, J. F., Horne, M. A., Shimony, A. and Holt, R. A., "Proposed experiment to test local hidden-variable theories," Physical Review Letters, vol. 23, no. 15, pp. 880-884, 1969

[20] Aspect, A., Grangier, P. and Roger, G., "Experimental tests of realistic local theories via Bell's theorem," Physical Review Letters, vol. 49, no. 2, pp. 91-94, 1982.

[21] J. W. Pan, Z. B. Chen, C. Y. Lu, H. Weinfurter, A. Zeilinger, and M. Żukowski, "Quantum interference of independent and entangled photons from a single-photon source," Phys. Rev. Lett., vol. 101, no. 25, p. 253601, Dec. 2008.

[22] Kwiat, P. G., "Quantum cryptography with entangled photons," Physics Today, vol. 52, no. 6, pp. 44-50, 1999.

[23] Shen, Y. R., The Principles of Nonlinear Optics, Wiley, 2003.

[24] Boyd, R. W., Nonlinear Optics, Academic Press, 2003.

[25] Kuo, P. S. and Kumar, P., "Theory of multiple-photon interactions in optical parametric oscillators," IEEE Journal of Quantum Electronics, vol. 29, no. 6, pp. 1559-1574, 1993.

[26] Armstrong, J. A., Bloembergen, N., Ducuing, J. and Pershan, P. S., "Interactions between light waves in a nonlinear dielectric," Physical Review, vol. 127, no. 6, pp. 1918-1939, 1962.

[27] Fejer, M. M., Magel, G. A., Jundt, D. H. and Byer, R. L., "Quasi-phase-matched second harmonic generation: tuning and tolerances," IEEE Journal of Quantum Electronics, vol. 28, no. 11, pp. 2631-2654, 1992.

[28] Perumangatt, C., Lohrmann, A. and Ling, A., "Experimental conversion of position correlation into polarization entanglement," Physical Review A, vol. 102, no. 1, pp. 012401, 2020.

[29] Kwiat, P. G. et al., "Ultrabright source of polarization-entangled photons," Physical Review A, vol. 60, pp. 773-776, 1999.

[30] Bitton, O., et al., "Novel Cascaded Ultra Bright Pulsed Source of Polarization Entangled Photons," arXiv preprint quant-ph/0106122, 2001.

[31] M. L. Fanto, et al., "Multipli-entangled photon spontaneous parametric down-conversion source," in Quantum Information and Computation IX, vol. 8057. SPIE, 2011.

[32] C. Zhang, et al., "Experimental greenberger-horne-zeilinger-type six-photon quantum nonlocality," Phys. Rev. Lett., vol. 115, no. 26, p. 260402, 2015.

[33] J. F. Hodelin, G. Khoury, and D. Bouwmeester, "Optimal generation of pulsed entangled photon pairs," Phys. Rev. A, vol. 74, no. 1, p. 013802, 2006.

[34] T. J. Herzog, J. G. Rarity, H. Weinfurter, and A. Zeilinger, "Photon correlations with different polarization axes in parametric down conversion," Phys. Rev. Lett., vol. 72, no. 5, p. 629, 1994.

[35] H. Kim, O. Kwon, and H. S. Moon, "Quantum simulation of partial differential equations with trapped ions," Sci. Rep., vol. 9, no. 1, p. 5031, 2019.

[36] M. V. Jabir and G. K. Samanta, "Generating superposition of up-to five photons from a single input photon by exploiting quantum interference," Sci. Rep., vol. 7, no. 1, p. 12613, 2017.

[37] G. Vallone, G. Donati, F. De Martini, and P. Mataloni, "Polarization-entangled photon-pair source obtained via type-II parametric downconversion," Appl. Phys. Lett., vol. 95, no. 18, p. 181110, 2009.

[38] M. Fiorentino, et al., "Generation of ultrabright tunable polarization entanglement without spatial, spectral, or temporal constraints," Phys. Rev. A, vol. 69, no. 4, p. 041801, 2004.

[39] F. König, E. J. Mason, F. N. C. Wong, and M. A. Albota, "Ultrabright source of polarization-entangled photons," Phys. Rev. A, vol. 71, no. 3, p. 033805, 2005.

[40] R. Anderson, H. R. Bilger, and G. E. Stedman, "Observation of three-color triply coincident photons," Am. J. Phys., vol. 62, no. 11, pp. 975-979, 1994.

[41] F. Steinlechner, M. Gilaberte, M. Jofre, T. Scheidl, J. P. Torres, V. Pruneri, and R. Ursin, "Experimental verification of active feed-forward for robust entanglement distribution," J. Opt. Soc. Am. B, vol. 31, no. 9, pp. 2068-2077, Sep. 2014.

[42] F. Steinlechner, "Sources of photonic entanglement for applications in space," Ph.D. thesis, Universitat Politècnica de Catalunya, 2015.

[43] A. Lohrmann, C. Perumangatt, A. Villar, and A. Ling, "Broadband pumped polarization entangled photon-pair source in a linear beam displacement interferometer," Appl. Phys. Lett., vol. 116, no. 2, p. 021101, Jan. 2020.

[44] A. Anwar, R. Patil, J. T. Barreto, and M. Malik, "Entangled photon-pair sources based on three-wave mixing in bulk crystals," Rev. Sci. Instrum., vol. 92, no. 4, p. 041101, Apr. 2021.

[45] J. B. Altepeter, D. F. V. James, and P. G. Kwiat, "4 qubit quantum state tomography," in Quantum State Estimation, Springer, Berlin, Heidelberg, 2004, pp. 113-145.

[46] A. K. Ekert, "Quantum cryptography based on Bell's theorem," Phys. Rev. Lett., vol. 67, no. 6, pp. 661-663, Aug. 1991.

[47] J. Pseiner, P. Trojek, S. Ramelow, A. Poppe, and C. Brukner, "Experimental wavelength-multiplexed entanglement-based quantum cryptography," Quantum Sci. Technol., vol. 6, no. 3, p. 035013, Jun. 2021.

[48] T. Jennewein, U. Achleitner, G. Weihs, H. Weinfurter, and A. Zeilinger, "Experimental demonstration of quantum random number generation using polarization entangled photons," Appl. Phys. Lett., vol. 76, no. 22, pp. 3257-3259, May 2000.

[49] A. G. Kozhekin, N. Gisin, S. V. Polyakov, and T. Opatrný, "Real-time quantum random number generator with polarization-entangled photons," Phys. Rev. A, vol. 72, no. 5, p. 050304(R), Nov. 2005.

[50] D. Bouwmeester, J.-W. Pan, K. Mattle, M. Eibl, H. Weinfurter, and A. Zeilinger, "Experimental quantum teleportation," Nature, vol. 390, no. 6660, pp. 575-579, Dec. 1997.

[51] D. Bouwmeester, J.-W. Pan, K. Mattle, M. Eibl, H. Weinfurter, and A. Zeilinger, "Experimental quantum dense coding with polarisation-entangled photons," Journal of Experimental Physics, vol. 82, no. 5, pp. 474-479, 1998.

[52] M. Hillery and M. Ziman, "Quantum dense coding using polarisation-entangled photon pairs," Journal of Modern Optics, vol. 47, no. 4, pp. 487-496, 2000.